Journal of Catalysis 284 (2011) 215–229

Contents lists available at SciVerse ScienceDirect

Journal of Catalysis

journal homepage: www.elsevier.com/locate/jcat

Brønsted acidity of amorphous silica–alumina: The molecular rules of proton transfer

Fabien Leydier [a,b], Céline Chizallet [a], Alexandra Chaumonnot [a], Mathieu Digne [a], Emmanuel Soyer [a], Anne-Agathe Quoineaud [a], Dominique Costa [b], Pascal Raybaud [a,*]

[a] IFP Energies nouvelles, Rond-point de l'échangeur de Solaize, BP3, 69360 Solaize, France
[b] Laboratoire de Physico-Chimie des Surfaces, CNRS-ENSCP (UMR 7045), ENSCP – Chimie-ParisTech, 11 rue Pierre et Marie Curie, 75005 Paris, France

ARTICLE INFO

Article history:
Available online 5 October 2011

Keywords:
Amorphous silica–alumina
Brønsted acidity
Density functional theory
Pseudo-bridging silanol
Infrared

ABSTRACT

The nature of acid sites on amorphous silica–alumina (ASA) is strongly debated, as well as their infrared signature. We report a combined experimental and computational study to unravel this challenging question at the atomic scale, focusing on proton transfer from ASA to lutidine (2,6-dimethylpyridine), an experimentally widely used molecule for probing Brønsted acid sites. The ASA surface model obtained by density functional theory (DFT) calculations is validated by the comparison of infrared frequencies of OH-groups with experimental spectra. The bands observed are assigned to the various OH-groups present, as a function of their hydrogen-bond donor character and of the proximity of silanols toward aluminum atoms. The affinity of lutidine (2,6-dimethylpyridine) for each site of the ASA surface is then evaluated by sampling the DFT model and varying the experimental pretreatment conditions. A general rule is established for Brønsted acidity of ASA, by comparison with calculations on reference silica, alumina, and mordenite models: the driving force for the proton transfer from OH-groups to lutidine is the stabilization of the conjugated base (after deprotonation) of the hydroxyls, more than the intrinsic acidity of the OH-group. Pseudo-bridging silanols (PBS) are thus found to be capable of proton transfer, thanks to the stabilization of silanolate species by the formation of additional O–Al and O–Si bonds. A prominent role of water molecules adsorbed on Al atoms is also shown: they act as a proton reservoir to express intrinsic acidity and to promote the acidity of neighboring silanols. Finally, we suggest that the $\tilde{\nu}_{8a}$ and the $\tilde{\nu}_{8b}$ modes of lutidinium species are inverted with regards to lutidine, contrary to what was previously thought on the basis of empirical data.

1. Introduction

Since the earlier use of amorphous silica–alumina (ASA) in the 1940s as acid catalysts [1,2], the variable acidity of these materials was the source of a significant interest and of very numerous questions. Formally, the composition of these materials can be written as a combination of silica (SiO_2), alumina (Al_2O_3), and eventually water (H_2O), depending on the synthesis and pretreatment conditions. Their amorphous nature however makes their structural resolution impossible, contrary to their zeolitic crystalline analogs. For this reason, and also due to the predominance of zeolites in the refining industry starting from the 1960s [1–3], the rationalization of the relationship between the structure of an acid site and its acidity was extensively performed on zeolite-type materials, both experimentally [4–8] and theoretically [9–11]. However, a renewed interest has recently been devoted to amorphous aluminosilicates [12–22], for several reasons. First, they generally exhibit milder acidity than zeolites, which enhances the selectivity for middle distillates in hydrocracking for example. Second, they gather both Lewis and Brønsted acidities, leading to numerous applications as supports for multifunctional heterogeneous catalysts. They are thus widely used in acid catalysis, from fine chemistry [23–27] to petrochemistry and refining [1], and biomass conversion [28,29]. ASA are also an alternative to the limited accessibility of acid sites, inherent to zeolite pore sizes, with respect to bulky reactants, products, or transition states. Moreover, ASAs are suspected as debris in (non-leached) de-aluminated zeolites [30–34]. Finally, due to their protonic conductivity, ASAs are also promising materials for electrolyte membranes in fuel cells [35].

From a fundamental point of view, the structure and behavior of their Brønsted acid sites are still questioned. The acidity of these materials strongly depends on the preparation mode and the Si/Al ratio [14,19]. FTIR was performed to attempt to identify bridging Si–(OH)–Al groups (Fig. 1a) of zeolitic type (typically, $\tilde{\nu}_{OH} = 3633$

* Corresponding author. Fax: +33 4 37 70 20 66.
E-mail addresses: fabien.leydier@ifpen.fr (F. Leydier), celine.chizallet@ifpen.fr (C. Chizallet), alexandra.chaumonnot@ifpen.fr (A. Chaumonnot), mathieu.digne@ifpen.fr (M. Digne), emmanuel.soyer@ifpen.fr (E. Soyer), anne-agathe.quoineaud@ifpen.fr (A.-A. Quoineaud), dominique-costa@chimie-paristech.fr (D. Costa), pascal.raybaud@ifpen.fr (P. Raybaud).

0021-9517/$ - see front matter © 2011 Elsevier Inc. All rights reserved.
doi:10.1016/j.jcat.2011.08.015

and 3567 cm^{-1} for Y [32]). On typical infrared spectra of ASAs [14], a narrow band at 3740–3745 cm^{-1} ($\tilde{\nu}_{OH}$ region) is observed, usually assigned to surface silanols. Depending on the pretreatment conditions, a poorly resolved broad band is centered around 3500–3600 cm^{-1}. On mesoporous ASA synthesized in the presence of a template, some authors managed to observe a thinner band around 3610 cm^{-1} in this region, which they naturally assigned to bridging Si–(OH)–Al groups (Fig. 1a) [36–39]. Many other authors do not support the existence of bridging Si–(OH)–Al groups, insofar as the 3600 cm^{-1} band is not well defined enough on their samples. They assign it to residual non-dissociated water, or to strongly hydrogen-bonded OH-groups, due to its disappearance upon thermal treatment [12–14,40–42]. On some alumina-based samples, the bands assigned to alumina OH-groups (around 3790, 3770, 3730, and 3600 cm^{-1}) are also observed [13,43].

The existence of zeolite-type bridging OH-groups on the ASA surface thus remains an open question. Some highly acidic OH-groups are identified by probe molecule adsorptions [12,14,18,38,39], isotopic exchange [20,21], and kinetic measurements [19,44]. Several hypotheses were formulated to explain this. Zeolite-like bridging OH-groups, whether observed or not by FTIR, are strongly suspected, due to the similar reactivity (intrinsic activation energy for a given – often very demanding – reaction, such as alkane cracking) of some sites in ASA and zeolites [19,44]. Hence, the different acidity of ASAs and zeolites would only be a matter of the Si–(OH)–Al site density. Alternatively, Gates et al. invoked silanols close to unsaturated Al atoms to be the Brønsted acid sites [45]. In the same spirit, Crépeau et al. [14] proposed silanols bonded to low-coordination aluminum atoms by a Si–O–Al bridge (Fig. 1b). We will call these sites Silanol–Al in the following. The "dynamic" behavior of silanols was addressed by Trombetta et al. [12]. On the basis of adsorption of nitrogenated probe molecules, they suggested that silanols in the vicinity of threefold-coordinated aluminum atoms could form an additional bond between the oxygen of the silanol and the threefold-coordinated aluminum atom (Fig. 1d). Later, Busca et al. [42] qualified this behavior as that of a "drawbridge" closing only in the presence of the molecule, as opposite to zeolites where it is permanently closed. Finally, Garrone et al. [46] also showed a strong acidity of water adsorbed on aluminum atoms (Fig. 1c), which was also supported by Williams et al. [41].

There is thus a need not only for a more accurate assignment of the FTIR spectra of ASA to unravel the nature of Brønsted acid sites, but also for a more rational understanding of the behavior of the acid sites, particularly in the presence of basic probe molecules. In a previous work [16,17], combining periodic density functional theory (DFT) calculations in periodic boundary conditions and force-field molecular dynamics, we proposed the first theoretical model of ASA surfaces, for various conditions of temperature and water partial pressure. These models exhibit various OH-groups. In particular, for hydroxyl coverage $\theta_{OH} \sim 5$–7 OH nm^{-2}, we pointed out remarkable sites: bridging Si–OH–Al analog to that of zeolites (Fig. 1a) but with an Al_V instead of Al_{IV}, as well as new sites called pseudo-bridging silanols (Fig. 1e and f). They consist of silanols in electrostatic interaction with acceptor Al atoms (PBS–Al) or silicon atoms (PBS–Si), but not covalently bonded to them as they are in zeolite sites.

In the present contribution, we combine FTIR experiments performed on a model ASA sample, and periodic DFT calculations, to establish the rules governing the Brønsted acidity of ASAs at the molecular scale. The sample and the DFT model were chosen so as to be as coherent as possible with respect to silication of alumina, Si/Al molar ratio, and OH content. We show first how our DFT model sheds new light on the assignment of infrared spectra of ASAs in the $\tilde{\nu}_{OH}$ region. Then, we propose a rationalization of the acidity of amorphous silica–alumina, by adsorption of 2,6-lutidine (2,6-dimethylpyridine, Scheme 1). Lutidine is a probe molecule usually devoted to the investigation of Brønsted acid sites [14,15,38,39,42,47–50]. Steric hindrance is indeed supposed to limit the interaction with Lewis acid sites, even if such interaction was also reported on various oxides [51], but in a much more limited manner than upon pyridine adsorption, for example. If the Brønsted acid site is strong enough to transfer its proton to lutidine, a lutidinium ion is obtained (Scheme 1).

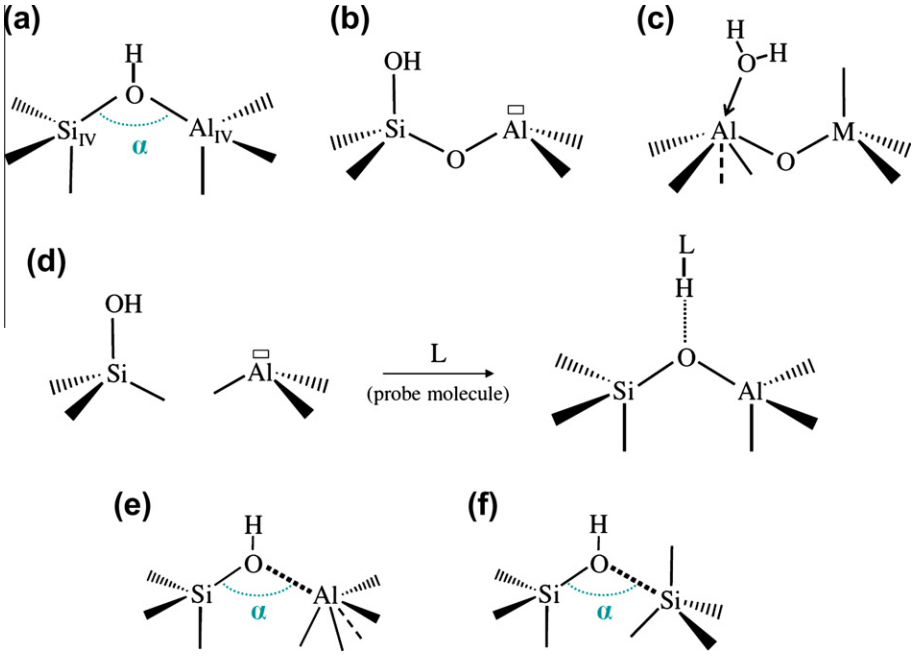

Fig. 1. OH-groups invoked at the surface of ASAs, models proposed from experiments (a–d) and DFT calculations (a, c, e, and f): (a) zeolite-like bridging Si–(OH)–Al group, (b) silanol in the vicinity of aluminum atoms [14], called silanol–Al in the following, (c) water molecules on Al atoms [41,46], (d) probe molecule induced bridging of specific silanols [12], (e) aluminic pseudo-bridiging silanols PBS–Al [16,17], (f) silicic pseudo-bridiging silanols PBS–Si.[17].

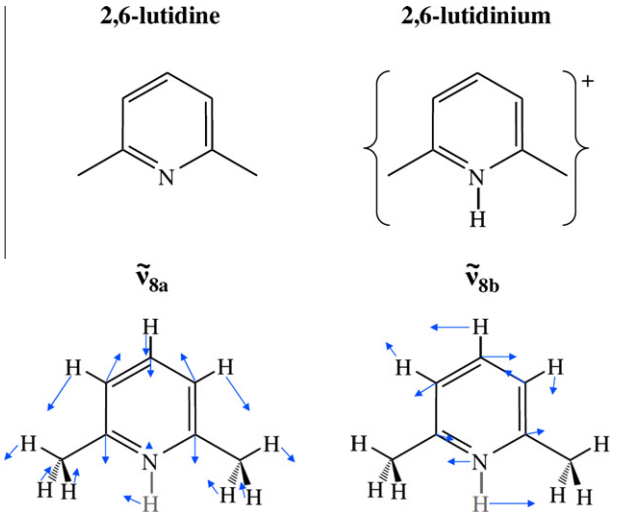

Scheme 1. Lutidine and lutidinium species, and their $\tilde{\nu}_{8a}$ and $\tilde{\nu}_{8b}$ vibration modes.

We also propose a computational assignment of infrared spectra of the adsorbed probe molecule, revealing new insights as compared to the well-admitted assignment [14,50–52]. This investigation leads us to a rational model of the origin of the acidity on ASA, by a comparison of our ASA models with reference computational systems such as pure γ-alumina [53,54], silica [55], and the mordenite (MOR) zeolite.

2. Experimental and computational methods

2.1. Samples

A silicated alumina sample was obtained by liquid-phase deposition of tetra-ethyl-orthosilicate (TEOS, $Si(OEt)_4$) on a mesoporous γ-alumina sample, with a protocol inspired from Refs. [43,45].

The starting γ-Al_2O_3 material is a powder sample provided by Axens with a high specific surface area of 350 $m^2\,g^{-1}$, a pore volume of about 1.2 $mL\,g^{-1}$, and a pore diameter centered at 8.5 nm. Then, 20 g of the γ-alumina sample was pretreated at 313 K for 4 h under vacuum (5 mbar), then stored under argon throughout the later grafting experiment. The sample was then put in contact with a large excess of TEOS (81.5 g, VWR, Rectapur 99%) in distilled and dried toluene (150 mL, VWR, Rectapur 99%). The grafting reaction was performed during 7 h under toluene reflux and magnetic stirring. The solution was then filtered, and the solid washed three times with distilled and dried toluene, which was then evaporated under argon flow for 4 h, then under vacuum (5 mbar) for 4 additional hours. The resulting powder was then hydrolyzed in water saturated vessel for 24 h, at room temperature, and dried in an oven at 393 K for 24 h. Finally, a calcination was performed for 4 h at 823 K (ramp: 2 K/min) under static air. The final product is characterized by a specific surface area of 287 $m^2\,g^{-1}$, a pore volume of about 0.9 $mL\,g^{-1}$, and a pore diameter centered at 6.8 nm.

The textural properties of the samples were analyzed by recording N_2 adsorption isotherms at 77 K, using a Micromeritics ASAP 2420 instrument. Before gas sorption analysis, the powder was pretreated for 4 h at 723 K under vacuum ($\sim 10^{-5}$ mbar). The specific surface area was determined using the Brunauer–Emmett–Teller (BET) model. Pore size distribution was estimated by applying BJH method to the desorption branch of isotherms. Finally, the pore volume was calculated at the maximum of P/P_0 value.

Elemental analyses were performed by X-ray fluorescence. The Si/Al molar ratio was estimated at 0.19 for the ASA sample, corresponding to 18 wt.% silica content, which is consistent with the ASA DFT model (Section 2.3).

2.2. FTIR characterizations

Infrared spectra were recorded on a Nexus Fourier transform instrument equipped with a KBr beam splitter and an MTC nitrogen-cooled detector. Infrared spectra of self-supporting pellets of pure powder sample, inserted in a IR cell (KBr windows) connected to a conventional gas manipulation evacuation line, were collected with 4 cm^{-1} resolution. The thermal treatment sequences applied to the sample are depicted in Scheme 2.

Each sample was then pretreated *in situ*, at the desired temperature T_1 (473, 573, or 773 K), for 10 h under vacuum ($\sim 10^{-6}$ mbar) with an intermediate step of 1 h at 423 K. The sample was then cooled down to room temperature, and lutidine (Aldrich, 99%) was adsorbed in excess (~10 mbar). The IR spectra are recorded during lutidine thermodesorption under vacuum ($\sim 10^{-6}$ mbar), after 2 h at 298 K, 1 h at 373 K, 1 h at 473 K, and 1 h at 573 K. The thermodesorption temperature will be noted T_2 in what follows. All spectra were then normalized according to the mass of the pellet and are presented for an equivalent mass of 20 mg.

2.3. DFT calculations

Density functional theory (DFT) calculations were performed using a periodic plane-wave method as implemented in the Vienna *Ab initio* Simulation Package (VASP 4.6) [56,57]. The exchange–correlation functional was treated within the generalized gradient approximation (GGA) parameterized by Perdew and Wang PW91 [58], and the electron–ion interaction was described by the projector augmented wave (PAW) scheme [59] with an energy cutoff of 500 eV to account for very accurate energies and geometries (convergence criterion: forces on relaxed atoms $<2 \times 10^{-2}$ eV $Å^{-1}$).

The harmonic O–H stretching frequencies were calculated numerically, with a displacement of ±0.005 Å around the equilibrium position of the OH vibrator. The anharmonicity corrections were performed by manual 1D exploration of the potential energy surface, along the axis determined by the O and the H atom, at constant position of the center of mass of the O–H vibrator, in the range [−0.3; +0.4 Å] around the equilibrium O–H bond length. Subsequently, the one-dimensional Schrödinger equation was solved numerically, based on a sixth-order fit of the potential energy curve, according to the method proposed by Lindberg [60], as implemented in the ANHARM module [61,62]. The harmonic vibration frequencies of lutidine were also evaluated numerically, with a displacement of ±0.05 Å around the equilibrium position of each atom of the lutidine molecule and of the nearest surface sites;

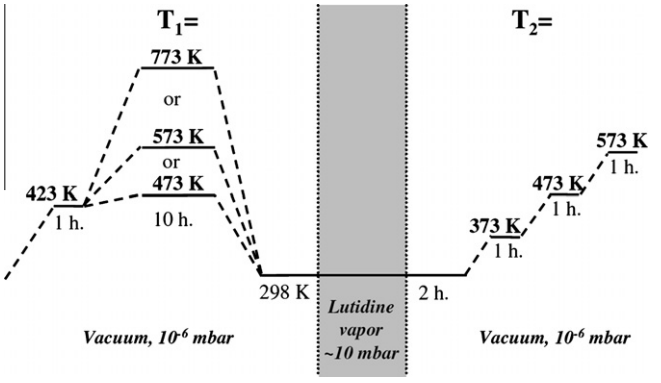

Scheme 2. *In situ* thermal treatment in the FTIR cell.

typically, the OH-group interacting with the molecule, the Si and/or Al atoms bonded to it and the second neighbor O atoms.

As described in details in [16], the ASA periodic surface model was obtained by simulating the contacting of a γ-Al_2O_3 (100) model [53,54] with a silica film, and the gradual hydration of the surface, for increasing water content [16]. For an alumina support with S_{BET} = 350 $m^2\ g^{-1}$ (as in our experiments), such a model corresponds to a silica content of 19 wt.%, in very good correspondence with the sample synthesized. Surface Si and Al atoms are named according to the same terminology as Ref. [16], U_i, V_i, X_i, Y_i, Z_i being Si atoms and I_i, II_i, III_i depicting Al atoms (Fig. 2). In typical experimental conditions, the surface models exhibiting θ_{OH} = 5.4 OH nm^{-2} (Fig. 2a) and θ_{OH} = 6.4 OH nm^{-2} (Fig. 2b) are considered to be representative of the diversity of acid sites on ASA obtained for thermal pretreatments close to experiments [17]. Indeed, 1.24 OH nm^{-2} (Ref. [63]) and 1 OH nm^{-2} (Ref. [14]) were reported for 723 K activated samples. An amount of 2.8–15 OH nm^{-2} was reported by Dorémieux-Morin et al. [64], depending on the dehydration temperature (up to 640 K) and chemical composition. In Ref. [65], by means of TGA data, a value of 4.8 OH nm^{-2} is found on one sample, which matches closely our model. These orders of magnitudes are comparable to the OH content of our model, but we may emphasize that experimental values depend tremendously on the synthesis method, the chemical composition, the calcination, and pretreatment temperatures of samples. Interestingly, these contents are close to that of a γ-alumina sample exhibiting mainly the (110) orientation [66].

The unit cell of ASA contains about 220 atoms, with cell dimensions of 11.13 × 16.77 $Å^2$ in the *x* and *y* directions (parallel to the surface), and *z* (perpendicular to the surface) up to 43 Å for lutidine adsorption studies. This allows the choice of a 2 × 1 × 1 K-points mesh. Dipolar correction was applied to account for the arbitrary interaction between asymmetric – thus polar – slabs. As compared to our previous works [16,17], the model exhibiting θ_{OH} = 5.4 OH mn^{-2} (Fig. 2a) was refined by *ab initio* molecular dynamics, at constant temperature (600 K), using the algorithm of Nosé (time step: 0.5 fs, total simulation: 1.5 ps, hydrogen atomic weight: 2 g mol^{-1}, Nosé mass: 2 atomic units) [67]. By quenching the most stable geometries, only one factor of stabilization of the system was found, consisting in the rotation of two OH-groups (Si(V_2)–OH and Si(U1)–OH, see Fig. 2a), slightly changing the hydrogen bond network.

The reference systems for pure alumina were taken from Refs. [53,54]. The γ-Al_2O_3 (110) (17.8 OH nm^{-2}, gamma point) and (100) (17.1 OH nm^{-2}, 2 × 1 × 1 *K*-points mesh) orientations were considered (see Supplementary material S2) in a strongly hydrated state to investigate the acidity of as many Brønsted sites as possible. For pure silicic system, the amorphous silica surface model of Tielens et al. [55] was chosen (5.8 OH nm^{-2}, see Supplementary material S1). Both alumina and silica systems were reoptimized (*K*-points mesh for the silica model: 2 × 1 × 1) with the same parameters as for ASAs, to achieve consistent comparisons. Model mordenite (with a main channel circumscribed by twelve-membered rings – 12 MR) was considered to depict the behavior of a typical proton-exchanged zeolite. The primitive cell, doubled in the *c* direction, was optimized (including lattice parameter relaxation) according to the same methods as ASA models. One T_4 site was substituted by an Al atom, with a proton in the O_{10} position (see for example Ref. [68] for structural details).

Adsorption energies $\Delta_{ads}U$ of lutidine were defined according to Eq. (1) ($U_{surf\text{-}Lu}$, U_{surf}, and U_{Lu} are the energies of the surface with and without lutidine and of the lutidine molecule, respectively).

$$\Delta_{ads}U = U_{surf-Lu} - U_{surf} - U_{Lu} \quad (1)$$

3. Results

3.1. IR spectra of the sample in the OH stretching vibration zone

The infrared spectra recorded after thermal pretreatment at T_1 = 473, 573, and 773 K (before any adsorption of lutidine) are depicted in Fig. 3a, in the O–H stretching frequency region. A main peak at 3743 cm^{-1} is observed. A large band around 3600 cm^{-1} is also present, as well as a shoulder at 3720 cm^{-1}. Note that the spectrum differs significantly from that of a γ-Al_2O_3 sample [69], but is more comparable to that of silica [70]. This trend is an indication that grafting of silica on alumina occurred during the preparation step and makes us confident in the good correspondence with our DFT model where no alumina-type OH-group remains.

3.2. Calculated features of OH-groups

3.2.1. Local structural properties of OH-groups

The main calculated geometric features of OH-groups present on the ASA model are reported in Table 1: O–H bond lengths, ∠Si–O···M (α) angles – see Fig. 1 – and O···M (M = Al or Si) distance for bridging OH-groups and PBS, H···O hydrogen bond lengths for hydrogen-bond donor groups. According to the DFT results, OH-groups present on the ASA surface models (Fig. 2) fall into six categories:

- One bridging OH-group, Al(III_3)-(OH)-Si(X_1) (Fig. 2b), very similar to that found in zeolites, except that Al(III_3) is pentacoordinated (and not tetracoordinated), and that the hydroxyl is hydrogen bond donor.
- Potential PBS–Al (Fig. 1e), which cannot be easily distinguished from standard silanols or silanol–Al, because many silanols in the vicinity of aluminum atoms (d_{O-Al} < 5 Å for example) can

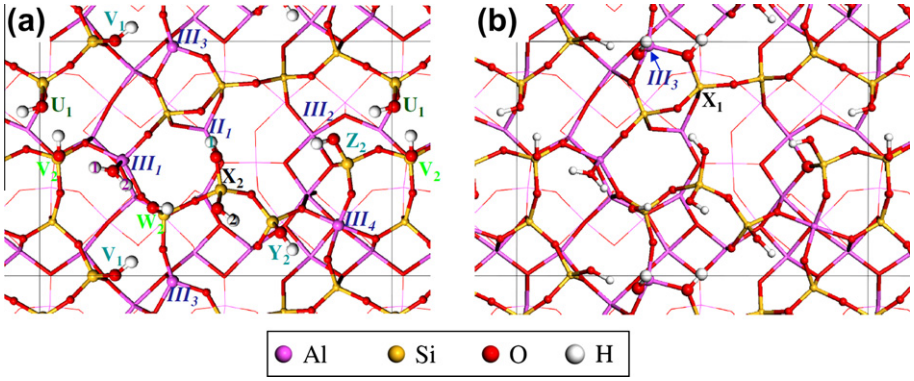

Fig. 2. ASA surface models (top views) for θ_{OH} = 5.4 nm^{-2} (a) and 6.4 nm^{-2} (b) according to Refs. [16,17]. The topmost slab of atoms is depicted in balls and sticks, the first and second underlying slabs in sticks and lines, respectively. The name of Lewis acid aluminum sites is depicted in blue, potential PBS–Al in dark green, silanol–Al in light green, proton of water molecules in purple, and silanol in black. (For interpretation of the references to colours in this figure legend, the reader is referred to the web version of this paper.)

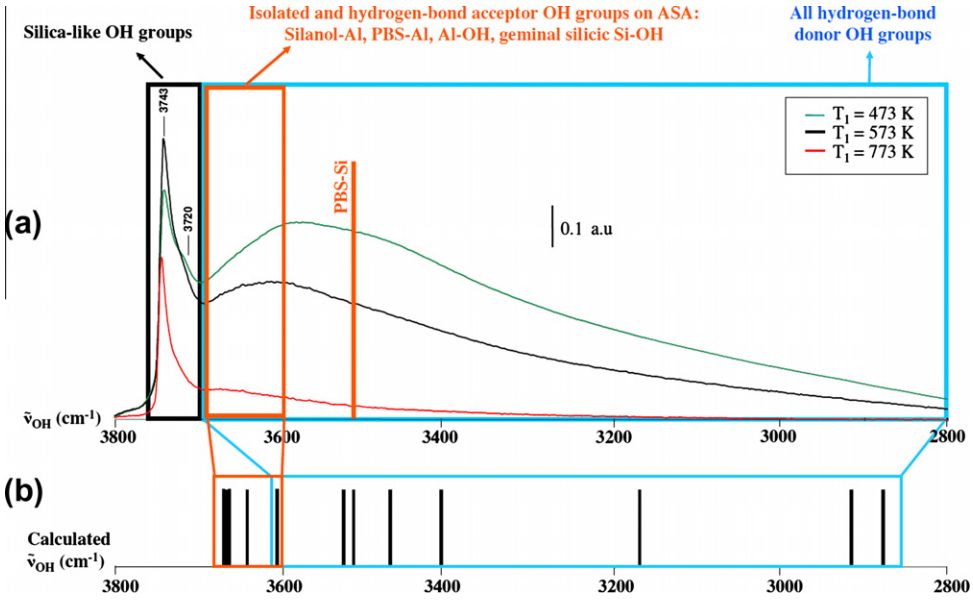

Fig. 3. (a) Experimental infrared spectrum of ASA, in the O–H stretching zone, for the ASA sample evacuated at T_1 = 473, 573, or 773 K. The assignment proposed is based on the computational results. (b) Calculated $\tilde{\nu}_{OH}$ for ASA. (For interpretation to colours in this figure, the reader is referred to the web version of this paper.)

Table 1
Hydroxyl groups present on the ASA surface model at 5.4 OH nm^{-2} (and 6.4 OH nm^{-2}), O–H bond length, Si–O···M (M = Si, Al) angles and O···M distances for bridging OH-groups and PBSs, hydrogen bond acceptor (*A*) or donor (*d*: weak, *D*: strong [a]) nature, hydrogen bond length for hydrogen-bond donor OH-groups, and calculated anharmonic O–H stretching frequency. See Fig. 2 for the position and terminology of OH-groups.

Type of site	Localization	O–H (Å)	α (°)	O···M (Å)	H bond	H···O (Å)	$\tilde{\nu}_{OH}$ (cm^{-1})
Bridging Si–OH–Al	Al(III$_3$)–(OH)–Si(X$_1$)*	1.012	122.2	1.940	*D*	1.912	2876
PBS–Si	Si(U$_1$)–OH···Si(V$_2$)	0.978	114.5	2.496	*A*	–	3514
Potential PBS–Al	Si(V$_1$)–OH···Al$_{IV}$ (III$_3$)	0.994	101.8	3.098	*D*	1.723	3169
	Si(Z$_2$)–OH···Al$_V$ (III$_2$)	0.971	67.0	3.441	*A*	–	3669
	Si(Y$_2$)–OH···Al$_V$ (III$_4$)	0.975	67.1	3.451	*d*	2.277	3606
	Si(X$_2$)–OH$_{(1)}$···Al$_{IV}$ (II$_1$)	0.979	92.5	4.640	*D*	1.862	3406
Silanol–Al	Si(W$_2$)–OH	0.973	–	–	*d*	2.266	3525
	Si(V$_2$)–OH	0.977			*d*	2.004	3667
Si–OH	Si(X$_2$)–OH$_{(2)}$	0.972	–	–	*A*	–	3641, 3681*
Al–OH	Al(III$_3$)–OH*	0.971	–	–	*A*	–	3665*
	Al(III$_1$)–HOH$_{(1)}$	0.980			*d*	2.024	3467
	Al(III$_1$)–HOH$_{(2)}$	1.008			*D*	1.627	2913

* ASA surface model at 6.4 OH nm^{-2}.
[a] The hydrogen-bond donor nature is called strong (*D*) when *d*(O···H) < 2 Å and weak (*d*) when *d*(O···H) > 2 Å. The limit for the absence of hydrogen bond is set to *d*(O···H) > 2.3 Å.

in principle be qualified of PBS–Al. Some of them are hydrogen bond donors (Table 1) toward neighboring oxygen atoms of the network. Establishing the key parameters to identify PBS–Al is one challenge of the present work.
- Some silanol–Al (silanols bonded to Al atoms via Si–O–Al bridges, similar to Fig. 1b) do not belong to the PBS–Al category (d_{O-Al} > 5 Å). They are indirectly bonded to Al atoms via Si–O–Al bridges, where the connecting O atom belongs to the surface network and not to any OH-group.
- One PBS–Si group (Fig. 1f) Si(U$_1$)–OH···Si(V$_2$).
- Silanols other than PBS or silanol–Al. This is the case of Si(X$_2$)–OH$_{(2)}$, which is far away from any Al atoms and not bonded to any Si–O–Al bridge.
- One water molecule adsorbed on an aluminum atom (III$_1$) is identified, and one Al–OH (Fig. 2b, Al(III$_3$)–OH) is also present at θ_{OH} = 6.4 OH nm^{-2}.

Accessible Lewis acid sites can also be reported as Al$_{IV}$(III$_3$) and Al$_V$(III$_4$).

3.2.2. Calculated vibrational properties of OH-groups

Calculated O–H stretching frequencies, including anharmonicity corrections, are reported in Table 1 and Fig. 3b for the various ASA sites. Analogous calculations were performed on the silica model (Supplementary material S1). Typically, for isolated or hydrogen-bond acceptor silanols on pure silica, the calculated $\tilde{\nu}_{OH}$ values are 3737–3655 cm^{-1} for terminal silanols and 3665–3700 cm^{-1} for geminal silanols. Experimentally, OH-groups on silica vibrate up to 3750 cm^{-1} [70], so we suspect to slightly underestimate the frequency values in our computational approach, by about 15 cm^{-1}. On ASA, the silica-like OH-groups vibrate at 3641–3681 cm^{-1} (calculated value), so generally slightly lower than on pure silica.

In line with their hydrogen-bond donor nature toward oxygen atoms of the ASA surface, the bridging Si–(OH)–Al group and several PBS exhibit very low stretching frequencies. The calculated values are in reasonable agreement with the observed frequency interval (Fig. 3), even if DFT calculations presumably underestimate stretching frequencies for hydrogen bond donor OH-groups, as known from the investigation of other solids [71,72].

As reported experimentally [73,74] and theoretically [55,72,75–77] for a wide range of solids, the stretching frequency is correlated with the O–H bond length (d(O–H), Fig. 4a), suggesting that it is closely linked to the OH bond strength. For hydrogen bond donor OH-groups, a monotonous variation is also observed for $\tilde{\nu}_{OH}$ as a function of the hydrogen-bond length (d(O···H), Fig. 4b), in a very analogous manner as reported in Ref. [73]. Strongly hydrogen-bond donors (D) exhibit higher sensitivity (larger slope) than weakly hydrogen-bond donors (d) (for which the curve is almost flat). The bridging Si–OH–Al group lies far away from the trend; it exhibits a much lower frequency than expected. This result shows that, apart from H bonding, the bridging nature (OH bonded at the same time to one Al and one Si atom) is a factor of strong frequency drop.

In the case of zeolites, a relationship was established between the O–H stretching frequency (or d_{O-H}, to which it is correlated) and the Si–O–Al angle of isolated bridging OH-groups (the higher the angle, the lower the frequency) [75,78–80]. Fig. 4c shows that surprisingly, such a correlation may also hold for PBS–Al and Si–(OH)–Al groups found on our model of the ASA surface, whatever the existence of strong or weak hydrogen bonding. However, the slope ($-13.5\ cm^{-1}/°$) is significantly larger than for zeolites (at most $-5\ cm^{-1}/°$ according to the data from Refs. [75,80]). Values reported in Table 1 show that the higher the Si–O···Al angle, the stronger the hydrogen bonding. These observations suggest that angle and hydrogen-bond effects lead synergistically to the correlation observed in Fig. 4c.

PBS–Si lies away from the correlation, its frequency being higher than expected, which can be easily rationalized by the fact that it is not hydrogen-bond donor. The slope relative to hydrogen-bond acceptors only (PBS–Si and Si(Z_2)–OH, dotted lines in Fig. 4c) is $-3.3\ cm^{-1}/°$, which is of the same order of magnitude than in zeolites. This shows that the neighboring Si atom in PBS–Si plays a role in the OH frequency, which is comparable to that of Al atoms for isolated PBS–Al and bridging OH-group.

3.3. Assignment of the spectra

On the basis of the calculations, we propose the assignment depicted in Fig. 3a and b. The frequencies higher than 3700 cm^{-1} are assigned to silica-like OH-groups, as no such higher values are ever calculated on the ASA model. The presence of aluminum in the neighborhood of silanols is thus clearly a first factor of frequency drop. If we except PBS–Si, all hydrogen-bond donor OH-groups exhibit lower frequencies (<3600 cm^{-1} according to calculations) than isolated or hydrogen-bond acceptor OH-groups. Considering that hydrogen-bond donor hydroxyls may exhibit much larger bands than other OH-groups, the whole experimental frequency range 2800–3700 cm^{-1} is likely concerned by their contribution. PBS–Si is an exception: although hydrogen bond acceptor only, it exhibits a quite low frequency (3514 cm^{-1}), suggesting a red-shifting role of the acceptor Si atom.

Finally, all other OH-groups on ASA vibrate between 3600 and 3700 cm^{-1} and are either isolated or hydrogen-bond acceptors (silanol–Al, PBS–Al, Al–OH, Si–OH). We expect that they give rise to a well-defined IR absorption peak. Thus, their signal may be hidden behind the broad band of the hydrogen-bond donor OH-groups. This explains why the blue and orange frames are overlapping in Fig. 3a.

Regarding the debated question on the existence of infrared signatures typical of zeolite-type bridging OH-groups, our results first show that the amount of such groups is very low as compared to other silanols, explaining their difficult observation. Then, their stability domain is reduced as compared to other types of OH-groups, according to our stability diagram (depicted in Ref. [16]). Finally, our DFT simulation shows that, on ASA samples, the bridging OH-groups are involved in strong hydrogen bonds, at the origin of the broadening of the corresponding band as compared to zeolitic OH-groups. In these conditions, it becomes very difficult to distinguish them from other hydrogen bond donor OH-groups.

3.4. Experimental investigation of lutidine adsorption and thermodesorption

Fig. 5a and b depicts the IR difference spectra after lutidine adsorption and thermodesorption at T_2 = 373, 473, and 573 K, of the ASA sample pretreated at T_1 = 573 K. The spectrum recorded before lutidine adsorption is subtracted from all spectra. In the O–H stretching zone (Fig. 5a), perturbed OH-groups can be identified. A negative band means that an interaction between the concerned OH-group and lutidine occurs. The absence of negative band does not necessarily mean the absence of interaction, as the decrease in the band can be compensated or exceeded by the increase in a new band. The 3743 and 3716 cm^{-1} bands are affected, which shows that silica-like OH-groups are interacting with lutidine. Moreover, a rather well-defined negative band is also observed around 3640 cm^{-1}, which can be assigned to silanol–Al and PBS–Al in particular (see Section 3.2). This suggests that below

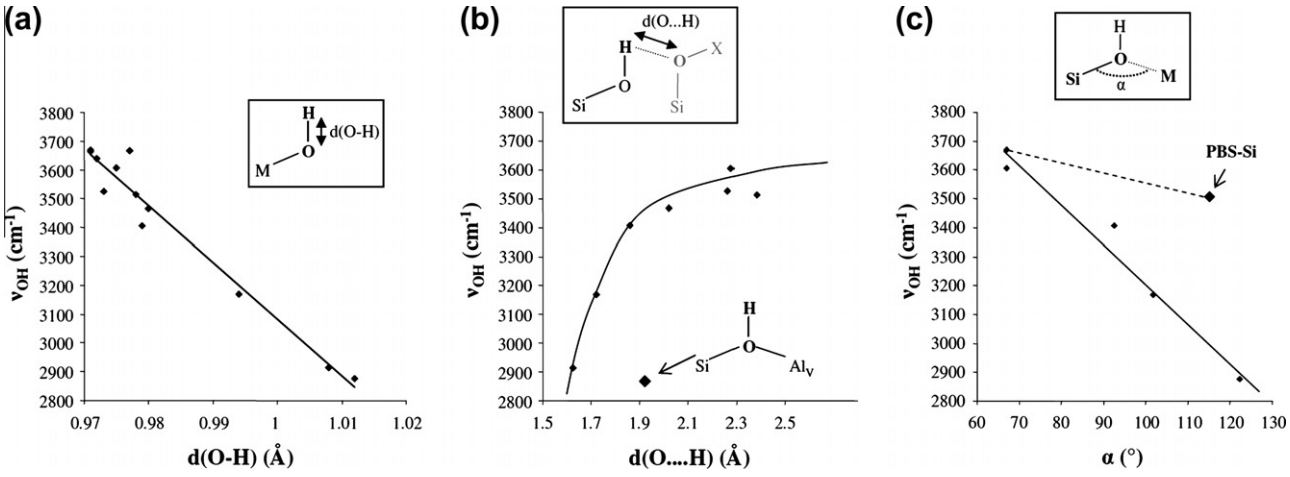

Fig. 4. Correlations between the calculated anharmonic O–H stretching frequency and (a) the O–H bond length, (b) the O···H hydrogen bond length for hydrogen-bond donor OH-groups to another O atom, either belonging to another OH-group or to the framework, and (c) the Si–O···M (M = Al, Si) angle.

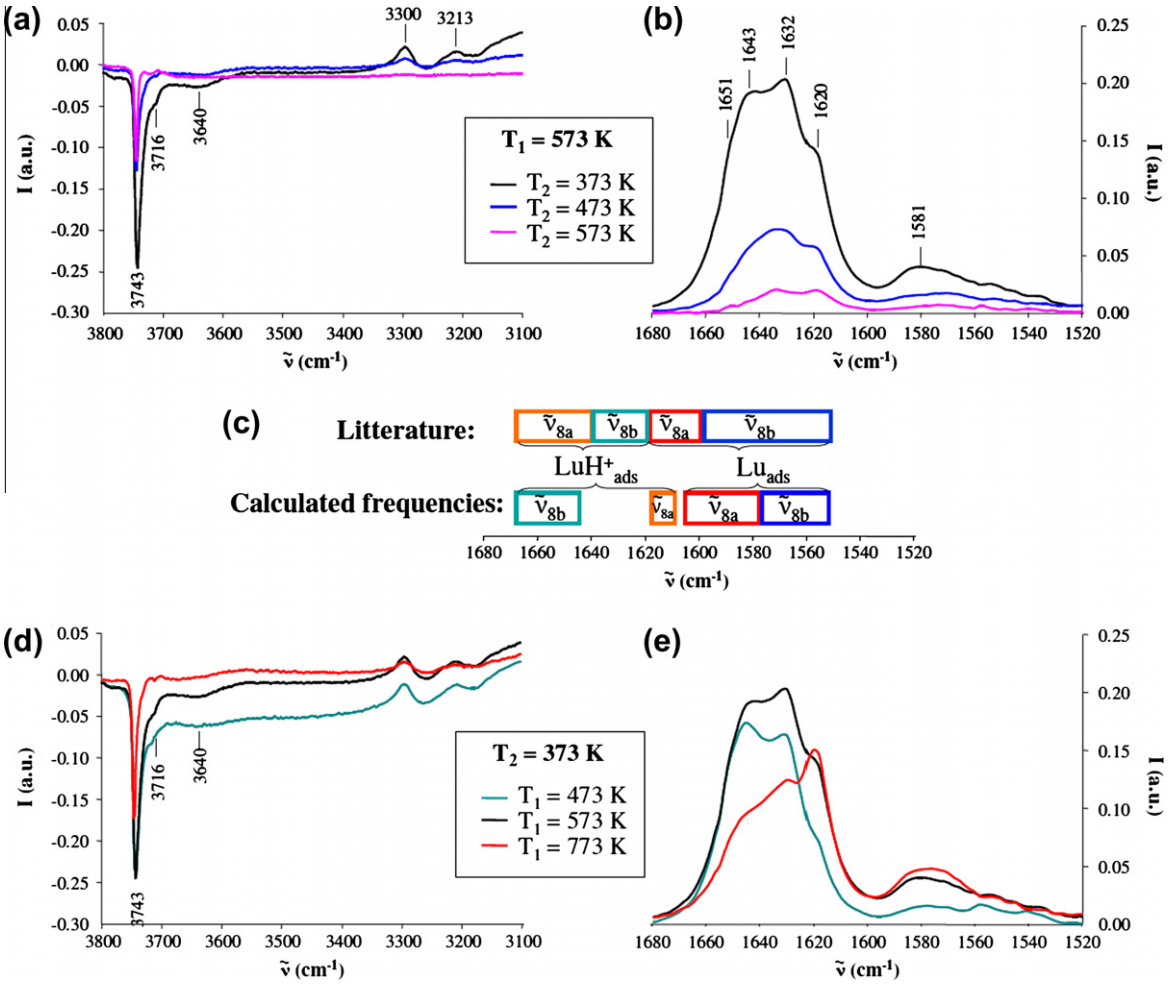

Fig. 5. (a and b) Infrared spectra of the ASA sample pretreated at T_1 = 573 K, recorded after lutidine adsorption and thermodesorption at T_2 = 373, 473, and 573 K. (a) O–H – and possible N–H – stretching zone, (b) ring stretching zone of the lutidine molecule. (c) Assignment of the 1520–1680 cm^{-1} zone, from the literature [14,50–52] and according to the present calculations. Lu_{ads} depicts lutidine adsorbed on Lewis acid sites and hydrogen-bonded to OH-groups (no proton transfer, contrary to LuH^+_{ads}). (d and e) Infrared spectra of the ASA sample pretreated at T_1 = 473, 573, and 773 K, recorded after lutidine adsorption and thermodesorption at T_2 = 373 K. (d) O–H – and possible N–H – stretching zone, (e) ring stretching zone of the lutidine molecule. (For interpretation to colours in this figure, the reader is referred to the web version of this paper.)

3700 cm^{-1}, acidic OH-groups are hidden by the main broad band of the spectrum, as suggested by exchange with deuterated benzene by Poduval et al. [21].

Positive bands appear at 3300 and 3213 cm^{-1}, as well as lower frequency bands that we will not comment as the C–H vibrations of lutidine typically appear below 3100 cm^{-1}. The 3300–3213 cm^{-1} bands can likely be assigned to a strongly hydrogen-bonded OH-group (presumably due to a strong interaction with lutidine) or to a N–H vibration of lutidinium after proton transfer. The evolution of their intensity as a function of T_2 (Fig. 5a) seems to be linked to that of the negative 3716–3640 cm^{-1} bands, which is consistent with the production of lutidinium species or strongly hydrogen-bonded OH-groups with lutidine, starting from OH-groups vibrating at 3716–3640 cm^{-1}. A thermodesorption at 573 K is moreover not sufficient to fully desorb lutidine from the surface, as shown by the nonzero signal in the corresponding difference spectra.

In the ring stretching zone of the lutidine molecule, two domains can be distinguished: the $\tilde{\nu}_{8a/8b}$ (1520–1680 cm^{-1}, Fig. 5b and Scheme 1) and the $\tilde{\nu}_{19a/19b}$ (1400–1500 cm^{-1}, not shown) zones. Being better resolved, the first one will be considered in the following. The assignment of the signal, as proposed in the literature [14,50–52], is depicted in Fig. 5c. It is inspired by the vibrational signature of the lutidine molecule in the liquid phase ($\tilde{\nu}_{8a}$ = 1605 cm^{-1}, $\tilde{\nu}_{8b}$ = 1580 cm^{-1} according to Ref. [48]), assuming that $\tilde{\nu}_{8a} > \tilde{\nu}_{8b}$ for all type of species. Physisorbed lutidine, as well as lutidine adsorbed through hydrogen bonding to OH-groups (Lu···HO) and to Lewis acid sites (Lu···Al), are noted Lu_{ads} in Fig. 5c. Their frequencies are expected at 1550–1600 cm^{-1} ($\tilde{\nu}_{8b}$) and 1600–1620 cm^{-1} ($\tilde{\nu}_{8a}$). When proton transfer from OH-groups to the lutidine molecule is possible, e.g., when sufficiently strong Brønsted acid sites are present, the frequencies are blue shifted, so that the frequencies of adsorbed lutidinium LuH^+_{ads} are expected at 1620–1640 cm^{-1} ($\tilde{\nu}_{8b}$) and 1640–1670 cm^{-1} ($\tilde{\nu}_{8a}$). In short, the assignment states that for a given species, the relation $\tilde{\nu}_{8a} > \tilde{\nu}_{8b}$ is maintained, but with systematically higher values for the lutidinium species than for adsorbed lutidine (without proton transfer). We will show in the following, thanks to the computational analysis that this assignment is fully justified, even if an inversion of the $\tilde{\nu}_{8a}$ and the $\tilde{\nu}_{8b}$ frequencies occurs for LuH^+_{ads} species in certain conditions.

In the 1600–1680 cm^{-1} zone, five main contributions can be deconvoluted (1650 ± 10, 1640 ± 10, 1630 ± 3, 1619 ± 3, and 1605 ± 10 cm^{-1}). Thus, bands between 1610 and 1660 cm^{-1} were integrated using five Gaussian curves (Fig. 6a). Upon increase in T_2, the signal decreases drastically. It indicates the loss of the adsorbed lutidine on the sample. Fig. 6b moreover shows that all components decrease as a function of the thermodesorption

temperature. This apparently contradicts chemical intuition, insofar as a more pronounced stability could be expected when proton transfer from OH-groups occurs (lutidinium) as compared to hydrogen-bonded lutidine to poorly acidic OH-groups. This surprising result will be rationalized by DFT calculations in what follows.

Finally, Fig. 5d and e depicts the impact of the pretreatment temperature T_1 on the nature of lutidine adducts on the ASA surface, for a thermodesorption temperature T_2 equal to 373 K. T_1 strongly influences the nature of the lutidine species present on the ASA surface (Fig. 5e). In particular, the temperature T_1 = 573 K seems to be the optimal pretreatment temperature to get the highest amount of OH-groups able to transfer their protons to lutidine (to produce lutidinium). Such species are much less abundant after treatment at T_1 = 773 K, which shows the limited thermal stability of OH-groups capable of proton transfer. Looking back at the nature of OH-groups present before adsorption of lutidine, Fig. 3a shows that between 573 and 773 K, most hydrogen-bond donors and silanols in the vicinity of aluminum and silicon atoms (silanol–Al, PBS–Al, and PBS–Si) have disappeared (frequencies lower that 3700 cm^{-1}). On the contrary, a significant intensity is still present at 773 K in the 3740 cm^{-1} area (Fig. 3a). This suggests that OH-groups vibrating at frequencies higher than 3700 cm^{-1} are not responsible for significant proton transfer to lutidine, whereas some of the OH-groups vibrating at frequencies lower than 3700 cm^{-1} are. This is confirmed by Fig. 5d, which shows that whatever the value of T_1, the OH-groups vibrating near 3745 cm^{-1} are almost equally perturbed, whereas the OH-groups vibrating at wave numbers lower than 3700 cm^{-1} are perturbed significantly only if T_1 < 773 K (for T_1 = 773 K, a small negative band remains around 3640 cm^{-1}, but its intensity is much lower than for T_1 < 773 K). Our previous calculations [16] showed that the thermally most stable OH-groups on the ASA surface are silanols and silanol–Al groups, whereas PBS, bridging OH-groups, and water molecules adsorbed on Al atoms disappear between 500 and 700 K. These theoretical and experimental observations suggest that Brønsted acid sites on ASA are of limited thermal stability (<773 K) and may belong to the PBS–Si, PBS–Al, bridging OH-groups, and/or water molecules adsorbed on aluminum atoms. Fig. 5e suggests that at T_1 = 773 K, lutidine interacts mainly with residual silanols (but without proton transfer) and Lewis acid sites, in agreement with the surface state found at this temperature by DFT calculations [16].

To conclude, among all operating conditions studied, the most appropriate one to enhance proton transfer is thus given by T_1 = 573 K and T_2 = 373 K (black spectra in Fig. 5). A detailed DFT investigation of the interaction of lutidine with the variety of OH-groups present on the ASA surface model is thus required to get a clearer view on the most acidic OH-groups.

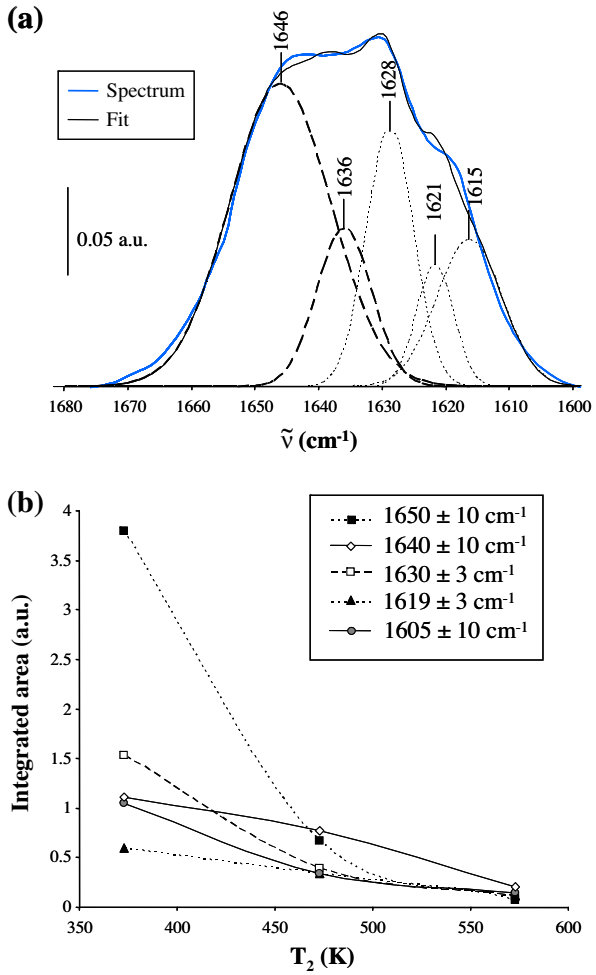

Fig. 6. (a) Decomposition of the 1600–1680 cm^{-1} signal, according to five contributions (after baseline correction), for the ASA sample pretreated at T_1 = 573 K, recorded after lutidine adsorption and thermodesorption at T_2 = 373 K. (b) Evolution of the area of the contributions as a function of the thermodesorption temperature T_2, for T_1 = 573 K.

3.5. Simulation of the lutidine/surface interaction

3.5.1. Adsorption energies, occurrence of proton transfer

The lutidine molecule was adsorbed on each hydroxyl group and potential Lewis acid site (prominent $Al(III_3)$, $Al(III_4)$, $Si(X_1)$, $Si(Z_1)$ atoms) of the ASA surface. Adsorption energies $\Delta_{ads}U$ are reported in Table 2 for ASA and in Supplementary material S2 for other solids (silica, alumina, mordenite). Note that the eventuality of proton transfer was carefully checked by forcing it, if it did not occur spontaneously.

On ASA, the interaction with Lewis acid sites was possible only on $Al(III_4)$, with moderate adsorption energy as compared to adsorption on other types of sites (−28 kJ mol^{-1}). This confirms the well admitted selectivity of lutidine for probing Brønsted acid sites. Moreover, in agreement with our experiments, proton transfer from hydroxyl groups to lutidine occurred in certain cases. Five OH-groups on the ASA surface model were able to transfer their proton to lutidine:

- The bridging Si–(OH)–Al group. However, the strength of the interaction (−34 kJ mol^{-1}) is lower than on a bridging OH-group in our mordenite model (−180 kJ mol^{-1}), where a proton transfer also occurs.
- A PBS–Al: $Si(V_1)$–OH···$Al_{IV}(III_3)$, which exhibits the highest Si–O···Al angle among PBS–Al on the model (Fig. 7a). This proton transfer occurs concomitantly with the formation of a new Al–O bond ($Al(III_3)$–O) between the newly formed silanolate and the acceptor Al atom.
- PBS–Si: $Si(U_1)$–(OH)···$Si(V_2)$ (Fig. 7b). This proton transfer is accompanied by the formation of a new Si–O bond ($Si(V_2)$–O) between the newly formed silanolate and the acceptor Si atom.
- One water molecule adsorbed on $Al(III_1)$: proton (n°2) (Fig. 7c).
- The $Si(W_2)$–OH group, which upon proton transfer to the lutidine molecule, catches one proton from the water molecule adsorbed on the neighboring Al atom (Fig. 7d). Water thus promotes the apparent Brønsted acidity of neighboring Si–OH-groups.

On the contrary, other PBS–Al exhibiting smaller Si–O···Al angles, silanol bonded to Al atoms *via* Si–O–Al bridges but for which the bridging of the silanolate on the Al atom is impossible (silanol–Al), and silanols far from the adsorbed water molecule

Table 2
Calculated adsorption energies, typical vibration frequencies of lutidine adsorbed on Brønsted and Lewis acid sites of ASA, with N–H distances and deprotonation energies. Data are given in italic when the lutidine molecule is protonated.

Type of site	Localization	$\Delta_{ads}U$ (kJ/mol)	$\tilde{\nu}_{8a(Lu)}$ (cm^{-1})[a]	$\tilde{\nu}_{8b(Lu)}$ (cm^{-1})[a]	d_{N-H} (Å)	E_{dep} (kJ mol^{-1})[c]
Bridging Si-OH-Al	$Al(III_1)$–(OH)–$Si(X_1)$[b]	*−34*	*1622*	*1605*	*1.030*	416
PBS - Si	$Si(U_1)$–OH···$Si(V_2)$	*−70*	*1615*	*1644*	*1.071*	444
Potential PBS – Al	$Si(V_1)$–OH···Al_{IV} (III_3)	*−45*	*1614*	*1653*	*1.096*	468
	$Si(Z_2)$-OH···Al_V (III_2)	−54	1596	1575	1.562	459
	$Si(Y_2)$-OH···Al_V (III_4)	−38	1586	1571	1.751	540
	$Si(X_2)$-$O_{(1)}$H···Al_{IV} (II_1)	−20	1587	1574	1.695	543
Silanol-Al	$Si(W_2)$-OH	*−66*	*1613*	*1663*	*1.091*	473
	$Si(V_2)$-OH	−49	1591	1572	1.596	463
Si-OH	$Si(X_2)$-$O_{(2)}$H	−44	1590	1572	1.661	521
Al-OH	$Al(III_1)$-$H_2O_{(1)}$	−46	1592	1571	1.560	454
	$Al(III_1)$-$H_2O_{(2)}$	*−35*	*1605*	*1657*	*1.122*	466
Lewis acid site	$Al(III_4)$	−28	1603	1570	–	–

[a] Frequencies of isolated species: – lutidine: $\tilde{\nu}_{8a} = 1579\ cm^{-1}$, $\tilde{\nu}_{8b} = 1571\ cm^{-1}$ (VASP calculation) – lutidinium: $\tilde{\nu}_{8a} = 1616\ cm^{-1}$, $\tilde{\nu}_{8b} = 1608\ cm^{-1}$ (VASP calculation).
[b] On the ASA surface model at 6.4 OH nm^{-2}.
[c] The values of deprotonation energies reported are artificially low for reasons explained in the text. Only the relative values should be compared.

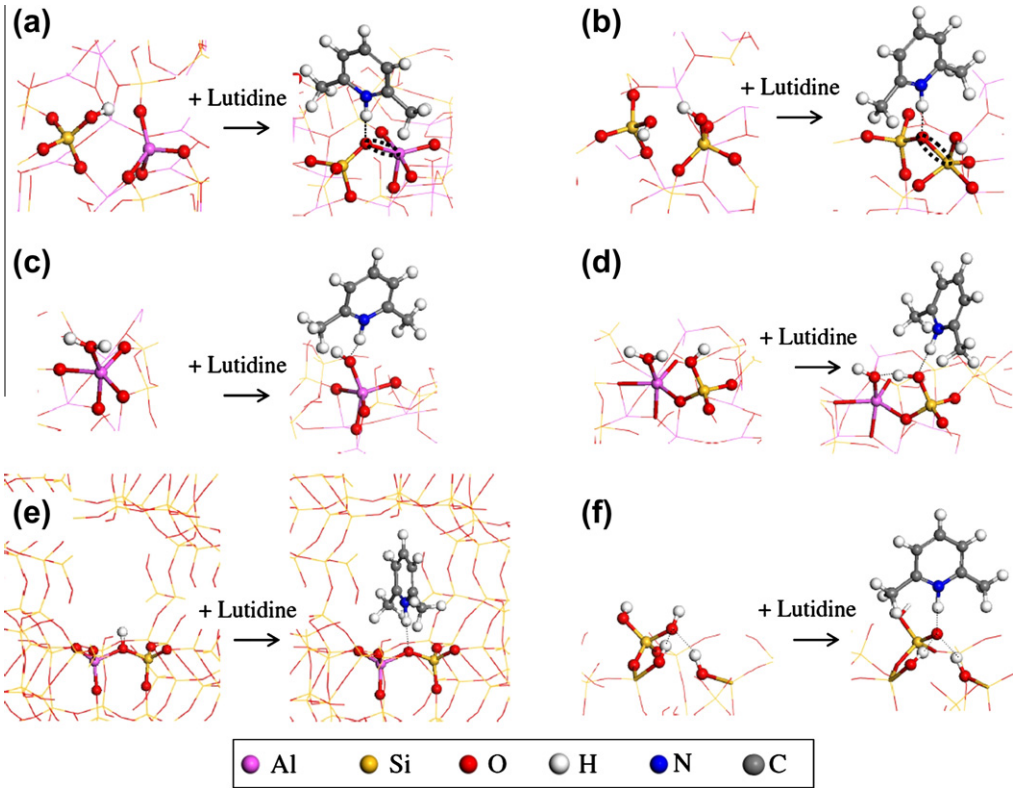

Fig. 7. (a–d) Deprotonation of hydroxyl groups of the ASA surface model by lutidine: (a) PBS–Al (V_1), (b) PBS–Si, (c) water molecule adsorbed on Al, (d) silanol next to the same water molecule, (e) bridging OH-group of mordenite, (f) proton transfer on the silica model. (For interpretation to colours in this figure, the reader is referred to the web version of this paper.)

could not protonate lutidine. Silanol–Al are thus acidic only when a water molecule is adsorbed on the neighboring Al atom. On the alumina surface, a single (and marginal) case of protonation of lutidine was found, in agreement with previously reported experiments demonstrating the absence (or very low amount) of any infrared band typical of lutidinium [49,51]. On the pure silica model, most OH-groups are not involved in any proton transfer, except two of them located in "silanol nests" (Fig. 7f). Indeed, the silanolate formed upon proton transfer is very close to two other OH-groups, playing the role of hydrogen-bond donors. Such a proton transfer on silica may however be marginal, as unprotonated lutidine species only were reported experimentally on silica [51,52].

These computational results are consistent with the experimental features reported in Section 3.4, insofar as upon adsorption of lutidine, we expect a decrease in the bands below 3700 cm^{-1} region, corresponding to PBS–Al, bridging OH-groups, PBS–Si, and water molecules adsorbed on Al atoms.

Finally, as shown in Table 2, there is no monotonous evolution between the proton transfer ability and adsorption energy. Indeed, proton transfer does not correspond to a stronger adsorption, except for PBS–Si and $Si(W_2)$–OH. This is explained by the strong hydrogen bond donor nature (Table 1) of PBS–Al and of the bridging OH-group, insofar as the adsorption energy also contains a contribution of the energy loss due to the hydrogen bond breaking. This absence of direct relationship between adsorption energy and proton transfer likely explains why all FTIR components of the 1520–1680 cm^{-1} band decrease simultaneously under thermodesorption of lutidine (Fig. 6b). Some of the lutidinium species

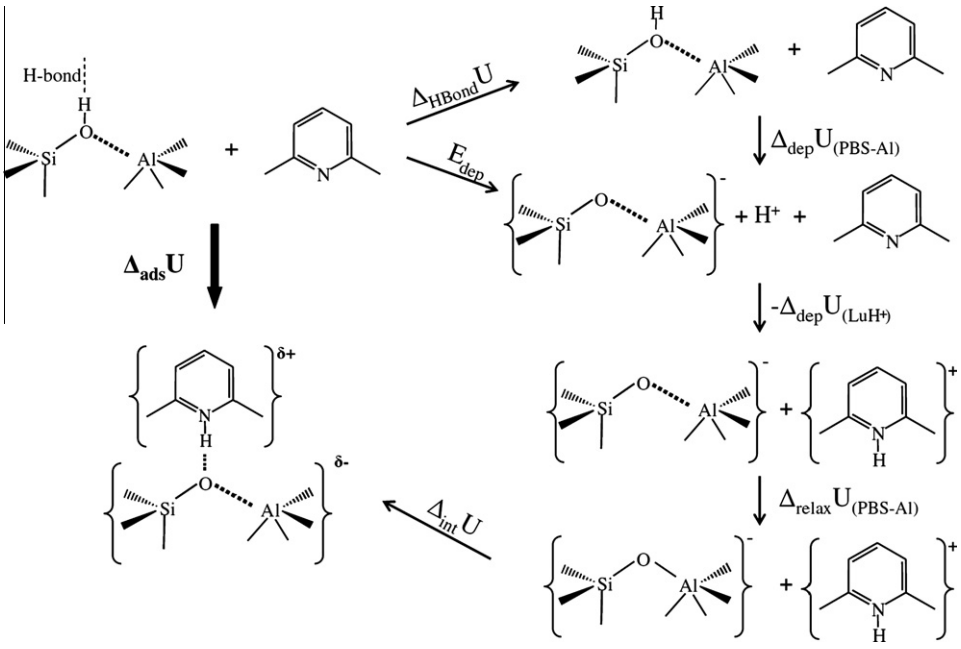

Fig. 8. Born–Haber cycle for the decomposition of the adsorption energy of lutidine on PBS–Al(V_1): hydrogen-bond breaking energy $\Delta_{HBond}U$, deprotonation energies of lutidinium and of PBS–Al (global E_{dep} and without hydrogen-bonding $\Delta_{dep}U$), relaxation energy of the silanolate $\Delta_{relax}U$, and energy of the interaction between LuH^+ and the bridge $\Delta_{int}U$.

are thus less stable than other hydrogen-bonded lutidine molecules.

3.5.2. Decomposition of the calculated adsorption energies

To better understand the origin of the adsorption energies and the factors governing proton transfer, the decomposition of the adsorption energy $\Delta_{ads}U$ into relevant contributions was performed. The example of PBS–Al (V_1) is depicted in Fig. 8. This OH-group is hydrogen-bond donor, so the hydrogen bond first needs to be broken before proton transfer. The corresponding energy cost for H bond breaking ($\Delta_{HBond}U$) was calculated by optimizing the position of the proton along the $N_{Lu}\cdots O_{OH}$ direction, but in the absence of lutidine. Then, the OH-group deprotonation energy $\Delta_{dep}U$ was calculated at constant geometry with VASP, by constraining the geometry of the deprotonated system and constraining the number of electrons to simulate the departure of H^+.

In the following, $E_{dep} = \Delta_{HBond}U + \Delta_{dep}U$ is the global deprotonation energy, taking into account the breaking of hydrogen bonds (but not the relaxation of the site after proton transfer). Note that VASP adds a positive charge as an homogeneous background, which is expected to stabilize by coulombic interactions the deprotonated – negatively charged – system considered in the calculations and artificially decreases the deprotonation energy. Thus, the values of E_{dep} reported in Tables 2 and 3 are significantly lower than values from the literature, calculated on non-periodic systems [80–83]. We shall only consider the relative E_{dep} values. The proton is then transferred to the lutidine molecule, with the energy $-\Delta_{dep}U(LuH^+) = +106$ kJ mol^{-1}. The relaxation energy of the surface site after deprotonation is given by $\Delta_{relax}U$. In the case of PBS-Al(V_1), this step corresponds to the formation of the Al–O bond from the silanolate. Finally, the lutidinium species and the relaxed deprotonated site are interacting, which stabilizes the system by $\Delta_{int}U$. Again, due to the stabilizing effect of the charged background imposed in the VASP calculation, $\Delta_{int}U$ is expected to be overestimated.

These data were calculated for a set of relevant systems (Table 3) and global deprotonation energies E_{dep} for all systems of the ASA surface (Table 2). It can be noted that small global deprotonation energy E_{dep} is not a relevant descriptor of an efficient proton transfer. Indeed, the E_{dep} value is lower for Si(V_2)–OH (a silanol–Al, not capable of proton transfer) than for the bridging OH-group of mordenite (capable of proton transfer). However, the highest E_{dep} values (>500 kJ mol^{-1}, Table 2) are found for OH-groups that are not capable of any proton transfer (Si(Y_2)–OH for example). So, high values of E_{dep} are a relevant indicator of poor proton transfer capacity. By contrast, for lower E_{dep}, this criterion is not sufficient to explain proton transfer.

As expected, hydrogen bonding of the hydroxyl groups impacts the overall energy balance up to ~25 kJ mol^{-1} only. This will also not be a key parameter determining proton transfer, since both $\Delta_{relax}U$ and $\Delta_{int}U$ are stronger contributors. In mordenite, regarding the Si–(OH)–Al group, $\Delta_{int}U$ completely counterbalances the high E_{dep} value. In a similar way as proposed in Ref. [84] for carbocations, this result can be explained by the electrostatic stabilizing contribution of the 12MR channel interacting with the lutidinium cation. Similar relaxation energies are found for the bridging OH-groups on MOR and ASA. However, $\Delta_{int}U$ is much more favorable in the former case, due to the stabilizing electrostatic effect of the mordenite three-dimensional framework, whereas the ASA surface is planar. Moreover, on ASA, the bridging OH-group lies parallel to the surface and about 2 Å under the mean OH-groups plane. Thus, its conjugated base is poorly accessible to the lutidinium species. This explains why, despite lower deprotonation energy, the acidity of the bridging OH-group is lower on ASA than in mordenite.

As compared to the bridging OH-group, PBS–Si and PBS–Al exhibit stronger adsorption due to $\Delta_{relax}U$ mainly, whereas $\Delta_{int}U$ remains as moderate as for the bridging silanol. This means that the stabilization of the silanolate by the formation of a new Si–O or Al–O bond is at the origin of their peculiar acidity. Thus, the stabilization of the conjugated base of the acid site plays a major role for the intrinsic acidity of the proton itself.

For Si(W_2)–OH (silanol–Al close to the water molecule adsorbed on Al atom), $\Delta_{relax}U$ is also significant. The stabilization of the silanolate by the formation of H–O bond (proton jump) is strongly beneficial. The absolute value of $\Delta_{int}U$ is also very high for this site, much higher than other sites on ASA. This suggests that the interaction of LuH^+ with the oxygen of a $Si–O^-$ species is stronger than

Table 3
Decomposition of the adsorption energy of lutidine for a set of OH-groups on the ASA model. The reported energies are defined in Fig. 8. All energy values are given in kJ mol^{-1}.

Site	$\Delta_{ads}U$	$\Delta_{HBond}U$	$\Delta_{dep}U$	E_{dep} [b]	$\Delta_{relax}U$	$\Delta_{int}U$ [b]
Bridging Si–OH–Al (MOR)	−180	0	496	496	−112	−670
Bridging Si–OH–Al (ASA)[a]	−34	–	–	416	−120	−435
PBS–Si	−70	6	438	444	−180	−441
PBS–Al (V_1)	−45	26	442	468	−181	−438
Si(W_2)–OH	−66	3	470	473	−161	−484

[a] For this site, the orientation of the OH-group to break hydrogen bonding is impossible due to local constraints.
[b] Values of deprotonation energies are artificially low, values of interaction energies are artificially high for reasons explained in the text (Section 3.5.2). Only relative values should be compared.

with a Si–O–Si or a Si–O–Al bridge from a closed PBS and even stronger than with the (ASA) bridging site. The accessibility of such an external silanol is likely at the origin of its stronger interaction with lutidine.

To summarize, we demonstrate that the intrinsic acidity of a proton is a necessary condition to obtain proton transfer, but the driving force for the deprotonation is the stabilization of the conjugated base of the acid site, together with its stabilizing interaction with the protonated basic molecule. This is true for ASA but also for zeolites as compared to ASA.

3.6. Calculated vibrational features of adsorbed lutidine

The calculated $\tilde{\nu}_{8a}$ and $\tilde{\nu}_{8b}$ modes for the adsorbed lutidine molecule are reported in Table 2 (and Fig. 5c). Calculated N–H and O–H stretching frequencies on ASA after lutidine adsorption are reported in Supplementary material S3. The very low values calculated for $\tilde{\nu}_{N-H}$ and $\tilde{\nu}_{O-H}$ (<3000 cm^{-1}) are consistent with the very low number of positive bands observed experimentally above 3000 cm^{-1} on the experimental difference spectra depicted in Fig. 5a and d. The calculated frequency interval for $\tilde{\nu}_{8a}$ and $\tilde{\nu}_{8b}$ modes (Fig. 5c) matches the experimental one (calculated values are harmonic). As compared to the previous assignments of the literature [14,51,52], our calculations confirm that the higher frequency contributions (1630–1650 cm^{-1}) can be considered as a proof of the occurrence of proton transfer from a surface site to the lutidine molecule (LuH^+_{ads}), whereas the lower zone (1550–1620 cm^{-1}) includes contributions of non-protonated lutidine (bonded to Al Lewis sites and OH-groups by hydrogen bonding). Moreover, we find that on the ASA surface, $\tilde{\nu}_{8a} < \tilde{\nu}_{8b}$ for the adsorbed lutidinium species, contrary to the usual statements, and contrary to gas-phase lutidine and adsorbed non-protonated lutidine species, for which $\tilde{\nu}_{8a} > \tilde{\nu}_{8b}$. Note that such an inversion was proposed on the basis of DFT computation for pyridinium species adsorbed on zeolite clusters by Castella-Ventura et al. [85].

To elucidate this inversion of modes for the ludininium species, we performed complementary molecular DFT calculations with the DMol^3 program [86] (PW91 functional, TNP basis sets) and found that the critical parameter for such inversion is the N–H distance within the lutidinium species (curves in Fig. 9a). Indeed, for large N···H distances (d_{N-H} > 1.37 Å, meaning lutidine far from H^+ species), $\tilde{\nu}_{8a}$ is greater than $\tilde{\nu}_{8b}$, as usually admitted. The same holds for the smallest N–H distances (d_{N-H} < 1.03 Å); for example, for the fully optimized geometry of isolated lutidinium (d_{N-H} = 1.02 Å). However, for intermediate distances, $\tilde{\nu}_{8a} < \tilde{\nu}_{8b}$. This is mainly due to the evolution of $\tilde{\nu}_{8b}$, whereas $\tilde{\nu}_{8a}$ follows a smooth and monotonic decrease with d_{N-H}. By nature, the $\tilde{\nu}_{8b}$ mode of lutidinium indeed strongly involves the N–H group, coupling with the N–H stretching mode (Scheme 1). This coupling is exalted at intermediate N–H distances (1.1–1.2 Å), explaining the high $\tilde{\nu}_{8b}$ values. On the contrary, the $\tilde{\nu}_{8a}$ mode mainly concerns CC bonds, which explains its lower sensitivity with regards to d_{N-H}. The

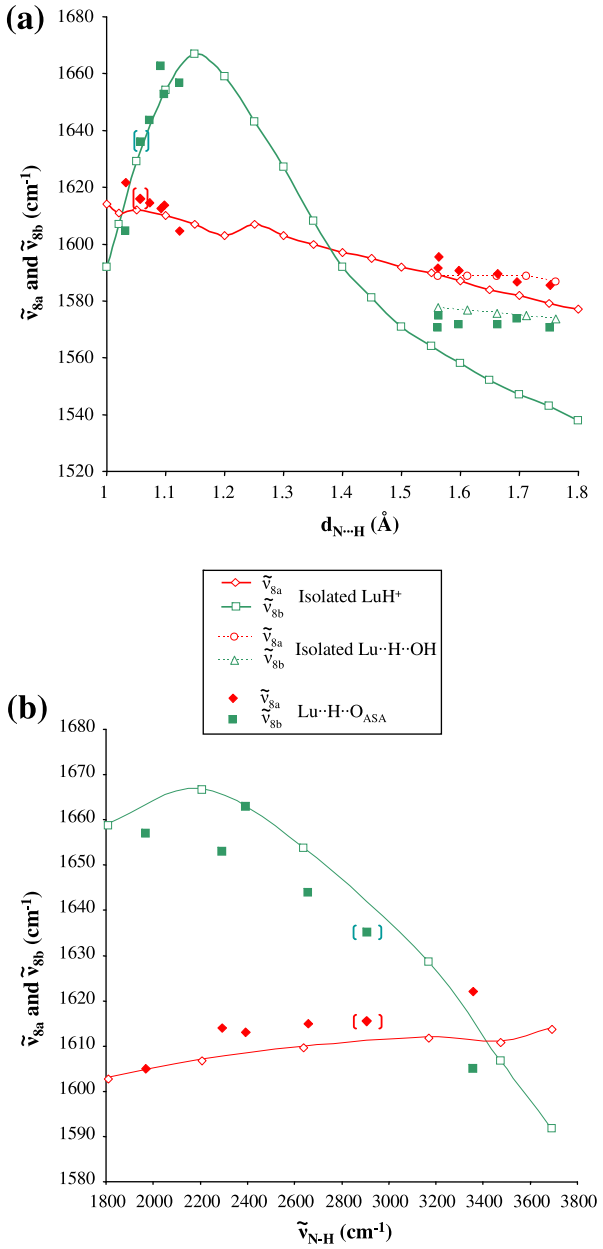

Fig. 9. (a) Calculated $\tilde{\nu}_{8a}$ and $\tilde{\nu}_{8b}$ frequencies, as a function of the N–H distance, for isolated lutidinium and for lutidine adducts on the ASA surface and on the MOR site (protonated or not). (b) Calculated $\tilde{\nu}_{8a}$ and $\tilde{\nu}_{8b}$ frequencies, as a function of $\tilde{\nu}_{NH}$, for the lutidinium species. Bold and dotted lines with empty symbols represent the DMol^3 calculations on isolated molecular systems. Full symbols represent the VASP calculations on ASA slab and MOR (full symbols with parentheses). (For interpretation to colours in this figure, the reader is referred to the web version of this paper.)

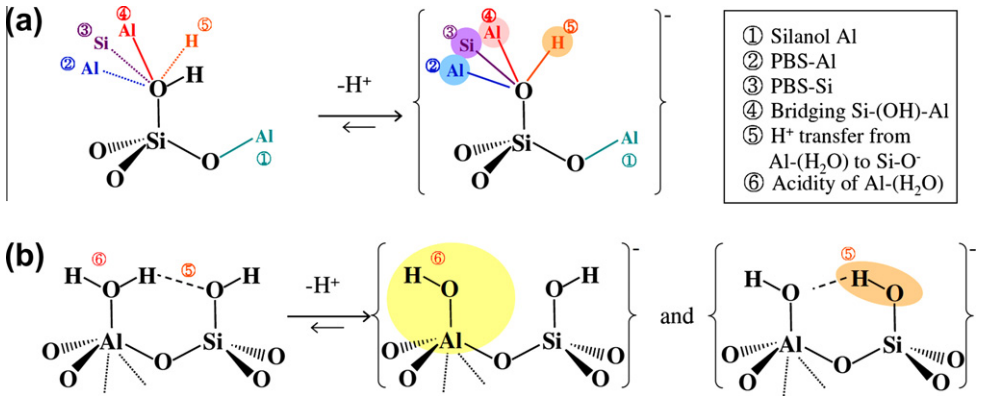

Fig. 10. Synopsis of the various Brønsted acid sites on the ASA surface: (a) Silanol–Al (①) does not stabilize the conjugated silanolate, thus, it is not deprotonated. PBS–Al (②) and PBS–Si (③) are deprotonated with the formation of new Al–O and Si–O bonds. Bridging OH-groups (④) are deprotonated thanks to the existence of the Al–O bond. Silanol in the vicinity of labile protons (⑤, see also (b)) is deprotonated with cascade proton transfer from the water molecule. (b) Acidity induced by water molecules adsorbed on Al atoms: proton transfer by the water molecule itself (⑥) or cascade proton transfer to the neighboring silanol (⑤, see also (a)). (For interpretation to colours in this figure, the reader is referred to the web version of this paper.)

geometry and frequency calculations performed with VASP for the ASA model follow the same trend (dots in Fig. 9a), with a reduced splitting of modes for large N···H distances (above 1.5 Å) as compared to the isolated lutidinium cation. This trend is fully rationalized by the presence of oxygen atoms on the surface, as shown by the calculation of an isolated Lu···H···OH system with DMol^3 (dotted lines in Fig. 9a).

Thus, we propose to invert $\tilde{\nu}_{8a}$ and $\tilde{\nu}_{8b}$ for protonated species in the assignment for IR spectra in this spectral zone, as depicted in Fig. 5c. On zeolites, Oliviero et al. reported that the $\tilde{\nu}_{8a}$ frequency decreases as the acidity of the site increases, measured by the $\tilde{\nu}_{N-H}$ frequency [49]. According to our results, this feature is typical of the $\tilde{\nu}_{8b}$ mode. Indeed, when proton transfer occurs ($d_{N-H} < 1.2$ Å), the longer d_{N-H}, the higher $\tilde{\nu}_{8b}$ (Fig. 9a). Long N–H distances likely characterize a strong interaction of lutidinium with the surface oxide ion that has been deprotonated, thus a strong basicity of the latter, which means a weak acidity for the original OH-group. Thus, we suggest that the $\tilde{\nu}_{8b}$ (and not $\tilde{\nu}_{8a}$) mode decreases as the acidity of the site increases, whereas the evolution of $\tilde{\nu}_{8a}$ is rather smooth but opposite. This is quantitatively depicted in Fig. 9b, with the decrease in $\tilde{\nu}_{8b}$ as a function of $\tilde{\nu}_{N-H}$. This is also explained by the fact that the lower $\tilde{\nu}_{N-H}$, the higher its coupling with $\tilde{\nu}_{8b}$, which frequency is thus increased. To conclude, our results on ASA compare well to the experiments of Oliviero et al. on zeolites, which validate our model and assignments, provided the assignments of the $\tilde{\nu}_{8b}$ and the $\tilde{\nu}_{8a}$ mode for the lutidinium species are inverted.

4. Discussion

4.1. General rules for Brønsted acidity of aluminosilicates

Fig. 10 provides a synopsis of all the surface sites leading to proton transfer with lutidine (efficient sites are colored). A very general molecular rule summarizing the Brønsted acidity of silanols on ASAs is thus deduced: direct or indirect interaction of silanols with aluminum (①, ②, and ④, Fig. 10a, left part) or silicon atoms (③, Fig. 10a, left part) may be beneficial for the exaltation of its acidity, but the most important factor determining deprotonation is the stabilization of the silanolate species obtained after proton transfer. Our results suggest that the extra negative charge on the silanolate cannot be efficiently stabilized on silanol–Al, so that no proton transfer occurs from these OH-groups. By contrast, the silanolate is stabilized on bridging OH-groups (as already known from zeolites), but also on PBS–Al and PBS–Si thanks to the formation of additional O–M bonds, provided the Si–O···M angle is large enough (higher than ~100°) and the O···M distance short enough (lower than ~3.4 Å). The presence of aluminum atoms in the silica network is thus a clear reason of enhanced Brønsted acidity of silanols as compared to silica.

The second source of Brønsted acidity on ASA comes from water molecules adsorbed on aluminum atoms. Provided they are not involved in strong hydrogen bonding with neighboring OH-groups, protons belonging to these water molecules can be transferred to basic molecules (⑥, Fig. 10b). If a strong hydrogen bond exists between the proton of such a water molecule and a neighboring silanol, Brønsted acidity arises from the silanol itself (⑤, Fig. 10a and b). The neighboring silanol is deprotonated by lutidine, and the conjugated silanolate relaxes by capturing a proton of the water molecule. The situation is equivalent to deprotonation of the water molecule, together with stabilization of the lutidinium species at the surrounding of a silanol instead of the Al–OH group. Such a process can be described as a "cascade proton transfer." It is strongly related to the hydrogen bond network, conditioning proton jumps between OH-groups, and to the aluminum content, aluminum atoms acting here as a reservoir of acidic water molecules.

In all cases, we showed that the clue for proton transfer on ASA is the stability of the conjugated base of the acidic hydroxyl group, more than the acidity of the hydroxyl *per se*.

4.2. Relevance of the model toward previous proposals

As mentioned in the introduction, several authors conclude to the existence of bridging Si–(OH)–Al groups as Brønsted acid sites on ASA [19,36–39,44]. In the present work, we substantiate the existence of such sites, through our DFT model validated by experiments. However, they are not the only sites capable of proton transfer.

The acidity of water molecules adsorbed on surface aluminum atoms was inferred by several authors [41,46]. Our work not only illustrates how such water molecules are directly deprotonated, but also anticipates that proton jumps from the adsorbed water molecules to neighboring silanols can also be a source of Brønsted acidity on ASA.

The behavior of PBS–Al groups meets the proposal of Trombetta et al. [12] (Fig. 2d), with the limitation that no Al_{III} are present on our model. But, we show that Al_{IV} can lead to a "drawbridge" behavior, to quote Busca et al. [42]. These PBS–Al sites explain why a specific role of Al_{IV} species was inferred in the acidity of ASAs [14,87].

To the best of our knowledge, the behavior of PBS–Si suggested in the present work is fully original in the context of the experimental elucidation of the ASA surface. The occurrence of Si_V is

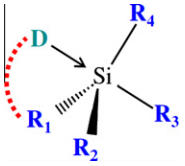

Scheme 3. Conditions of formation of a Si_V.

indeed very scarce as compared to the most usual tetravalent state and induced strong interest mainly in three following fields: geochemistry, fluorinated oxides, and molecular coordination chemistry. Indeed, high pressures and/or the presence of non-bridging oxygens (NBOs) are at the origin of Si_V in geological glasses [88–90]. Synthesis of zeolites or silica in fluorinated medium can lead to $[SiO_{4/2}F]^-$ units [91–95]. A set of molecular complexes containing Si_V was also reported [96–98]. We can identify three factors (Scheme 3) that can enhance the formation of Si_V:

1. *Electronegative ligands* in the tetracoordinated state (R_{1-4}), so as to increase the electrophilicity of the silicon toward additional nucleophilic species. In organic complexes, fluorine [99–101] very often plays this role, as most electronegative elements. On the ASA surface, Si–O–Al bridges induce such an effect, Al^{3+} being a Lewis acid.
2. *High nucleophilicity* of the *D* (for Donor) species, which plays the role of the fifth ligand. Amines [102] or alkoxides [100,103,104] can behave so in molecular complexes. The fluoride ions play this role in fluorinated zeolites or silica [91–95]. In amorphous geological silicates, the abundance of NBOs, to which higher nucleophilicity is assigned as compared to bridging oxygens (belonging to Si–O–Si bridges), was correlated with the occurrence of Si_V [105]. On ASA, as already discussed, the $Si–O^-$ species generated after deprotonation of a silanol is intrinsically highly unstable. Such an electrophilic species is thus a good candidate to allow the formation of Si_V (and Al_V) species.
3. *Geometric constraints* will finally force the electrophilic silicon atom and the nucleophilic D species to collapse. Such a condition is obtained on molecular complexes by chelation, i.e., grafting the *D* species on a multidentate ligand R_4 for example [101,104,106,107], whereas high pressures as found in the Earth's mantle are most of the time necessary to induce Si_V in geological silicates [88,90]. On the ASA surface, silicon atoms are in much more constrained environment than on silica. This can be quantified by the higher density of gamma alumina, resulting in a higher bulk modulus (162 GPa [108]) as compared to amorphous silica (11.5 GPa for alpha-cristobalite [109]). The alumina matrix thus induces an artificial external pressure on the silicon atoms, which will be more likely to convert in the pentacoordinate state, even at ambient pressure.

These three factors are thus gathered on the ASA surface after deprotonation of PBS–Si and explain why such a process may be invoked on the ASA surface and not on pure silica.

4.3. Generalization to other classes of ASA materials and to reactions of catalytic relevance

Our model was built from a gamma alumina model on top of which silica derivates were deposited [16]. After a sequence of calculations aiming at reproducing thermal treatments, a silica surface enriched model is obtained, supported on bulk alumina. Conventional ASA catalysts are sometimes richer in Si than in Al and are not necessarily synthesized from alumina. However, we expect our model to be transferable (to some extent) to several classes of ASA materials. Indeed, the very top surface plane of our model is much richer in Si than in Al (Si/Al = 4), even if the lower layers are composed of alumina only. So qualitatively, we do not expect significantly different sites to be exposed on silica-rich samples. The chemical features that could differ between alumina-based and silica-rich samples are typically:

- The relative amounts of Al_{IV}, Al_V, and Al_{VI} in the samples. This may impact the amount and nature of various types of PBS–Al: a higher population of PBS–Al_{IV} may be present on the silica-rich samples, as compared to PBS–Al_V or PBS–Al_{VI}. Note that the most efficient PBS–Al on our model is indeed a PBS–Al_{IV}. This may also lead to Al_{IV}–(H_2O) groups, whereas in the present study, we focus on a Al_V–(H_2O). Finally, our model exhibits one bridging Al_V–(OH)–Si, whereas on silica-rich samples, Al_{IV}–(OH)–Si sites may be statistically more easily found. All these factors could be a source of exalted Brønsted acidity for silica-rich samples.
- The surface strain induced by the alumina substrate on the silica layer, which is absent for silica-rich samples (provided no alumina domains are formed, which strongly depends on the synthesis procedure). Such a strain is expected to contribute to the proton transfer from PBS–Si. Thus, the behavior of PBS–Si might not be observable for all Si/Al ratios.

Moreover, the present work deals with the behavior of ASA in contact with the lutidine probe molecule, which is not a true reactant molecule such as a hydrocarbon molecule that exhibits a weaker basicity. Proton transfer is the first step of most acid-catalyzed reaction. The protonation of an alkene or of an aromatic molecule will similarly involve the stabilization of the conjugate base of the acid sites. However, if the proton transfer ability of a surface site is the first condition for an acid–base catalyzed reaction, it is not the unique relevant parameter. Considering for instance an alkene, after proton transfer, a carbocation may be formed by analogy with what occurs in zeolites. The energy profile of the formation of this species will be different from that generating lutidinium from lutidine. On the one hand, the two molecules exhibit different basicities; on the other hand, there is a competition between the stabilization of the carbocation and the alkoxy species [6,11,110–112]. This process is more complex for hydrocarbons than for lutidine and could thus counterbalance the stabilization energy of the silanolate by other atoms from the framework (Al for PBS–Al, Si for PBS–Si, H for cascade proton transfer). Finally, the kinetics of the transformation of the carbocation (oligomerisation, isomerization, cracking, etc.) will also have a role on the global reactivity of the sample, not only the first proton transfer step.

Note that aromatic species, leading to arenium Wheland intermediates after protonation, will likely give rise to quite different behavior than carbocations issued from the protonation of alkenes. For example, H/D exchange of C_6D_6 with surface OH-groups was investigated on ASA by Poduval et al. [21]. The authors observe the growth of three bands below 2700 cm^{-1}, which they assign to bridging Si–(OD)–Al groups. However, only the similarity with IR spectra obtained on USY suggests that they are zeolite-like. In fact, the atomic structure of those sites can still be questioned, and we cannot exclude the existence of PBS in USY. Our results do not exclude that they could indeed be zeolite-like bridging acid sites, as invoked by Poduval et al. The bridging site modeled in our present study is not an optimal site (in terms of lutidine adsorption energy), because it is sterically hindered by hydrogen bonds. We suspect that this site would not be more favorable for the activation of aromatic species. However, the samples used by Poduval et al. are silicon rich, which could change its acidity as discussed previously (Al_{IV}–(OH)–Si instead of Al_V–(OH)–Si). Finally, we cannot exclude that PBS–Si, PBS–Al, water molecules, or silanols are

also present in the bands assigned to OD bridging sites by Poduval et al. In that case, they could thus take part to the correlation they observe between H/D exchange followed by FTIR and catalytic activity in hydroconversion of *n*-heptane.

5. Conclusion

Considering the very much debated acidity of amorphous silica–alumina (ASA), we undertook a combined experimental and computational study to elucidate the nature of the Brønsted acid sites and their specific behavior with regards to proton-acceptor molecules. We focused on proton transfer from surface OH-groups to 2,6-dimethylpyridine (2,6-lutidine), which is considered as a probe specific to Brønsted acid sites. Experimentally, a model sample obtained by the grafting of tetraorthosilicate on γ-alumina (18 wt.% silica) was chosen, and the adsorption of lutidine was monitored by infrared spectroscopy. Theoretically, the ASA model obtained by the deposition of silica onto γ-alumina (equivalent to 19 wt.% silica) was studied by density functional theory calculations. The OH content (5–7 OH nm^{-2}) of the model was adjusted to the experimental operating conditions. In particular, this model highlighted original OH-groups called pseudo-bridging silanols (PBS).

DFT calculations led to the proposal of an assignment of the FTIR spectra, first in the OH stretching region: isolated silanols in a purely silicic environment are responsible for frequencies higher than 3700 cm^{-1}, whereas isolated and hydrogen-bond acceptor Si–OH close to Al atoms (through space – PBS–Al – or through Si–O–Al bridges – silanol–Al) vibrate between 3600 and 3700 cm^{-1}. Silicic pseudo-bridging silanols (PBS–Si) are expected around 3515 cm^{-1}. A large band between 2800 and 3700 cm^{-1} contains the contributions of all hydrogen bond donor OH-groups, irrespective of their chemical nature.

Upon lutidine adsorption, vibrational properties of several types of OH-groups from the ASA sample are affected, in particular those vibrating at 3740, 3720, and 3640 cm^{-1}. The analysis of the aromatic ring vibrations of lutidine suggests the coexistence of lutidinium species, obtained by proton transfer from surface OH-groups to lutidine, and lutidine maintaining hydrogen bonds with less acidic OH-groups. The thermal stability of lutidinium species is not systematically higher than that of hydrogen-bonded species. DFT calculations indeed show that proton transfer occurs from several types of OH-groups. Decomposition of the adsorption energy of lutidine and comparison with adsorption on pure γ-Al_2O_3, pure SiO_2 and zeolitic models lead to general rules to explain such proton transfer. The general condition to promote proton transfer is thus the stability of the conjugated base of the Brønsted acid site, more than the intrinsic acidity of the acid site itself. In practice, pseudo-bridging silanols (PBS–Al and PBS–Si) are capable of proton transfer, thanks to the stabilization of silanolate species by the formation of additional O–Al and O–Si bonds. A prominent role of water molecules adsorbed on Al atoms is also demonstrated: they play the role of proton reservoir to express intrinsic acidity (the conjugated base is then a stable Al–OH) and to promote the acidity of neighboring silanols thanks to a cascade proton transfer.

This behavior is different from bridging Si–(OH)–Al groups found in zeolites and on ASA, for which stabilization is not due to relaxation effects but rather to electrostatic stabilization of lutidinium on the deprotonated site. This is particularly pronounced for zeolites.

Finally, the assignment of the infrared spectra of adsorbed lutidine and lutidinium in the aromatic ring vibration zone was revisited thanks to our DFT calculations. An inversion of the $\tilde{\nu}_{8a}$ and $\tilde{\nu}_{8b}$ modes was indeed revealed for adsorbed lutidinium as compared to lutidine. The N–H distance (N from lutidine, H from the OH-group) was found to be the critical parameter justifying this inversion.

Thus, through a combined spectroscopic and DFT investigation, we established rational atomistic rules for the conditions allowing proton transfer from ASA. This work is the first step toward the understanding of the reactivity of such a complex acid solid. We will then aim at understanding the impact of this Brønsted acidity on the reactivity of the solid toward reactive molecules.

Acknowledgments

The authors thank Prof. J. van Bokhoven (ETH Zürich) and S. Rafik-Clément (IFPEN) for fruitful discussions and help in the synthesis of the samples. F. Tielens (Paris 6 University) is acknowledged for providing us the silica surface model. All calculations were performed at IFPEN HPC center and at IDRIS/CINES HPC centers within projects x2010086134 and x2011086134 funded by GENCI.

Appendix A. Supplementary data

Supplementary data associated with this article can be found, in the online version, at doi:10.1016/j.jcat.2011.08.015.

References

[1] C. Marcilly, Acid–Basic Catalysis, Technip, Paris, 2005.
[2] H. Hattori, Top. Catal. 53 (2010) 432.
[3] W. Vermeiren, J.P. Gilson, Top. Catal. 52 (2009) 1131.
[4] D. Barthomeuf, J. Phys. Chem. 83 (1979) 249.
[5] W.O. Haag, R.M. Lago, P.B. Weisz, Nature 309 (1984) 589.
[6] A. Corma, Chem. Rev. 95 (1995) 559.
[7] G. Busca, Chem. Rev. 107 (2007) 5366.
[8] A. Bhan, E. Iglesia, Acc. Chem. Res. 41 (2008) 559.
[9] J. Sauer, Chem. Rev. 89 (1989) 199.
[10] R. van Santen, G.J. Kramer, Chem. Rev. 95 (1995) 637.
[11] J. Hafner, L. Benco, T. Bucko, Top. Catal. 37 (2006) 41.
[12] M. Trombetta, G. Busca, S. Rossini, V. Piccoli, U. Cornaro, A. Guercio, R. Catani, R.J. Willey, J. Catal. 179 (1998) 581.
[13] W. Daniell, U. Schubert, R. Glöckler, A. Meyer, K. Noweck, H. Knözinger, Appl. Catal. A 196 (2000) 247.
[14] G. Crépeau, V. Montouillout, A. Vimont, L. Mariey, T. Cseri, F. Maugé, J. Phys. Chem. B 110 (2006) 15172.
[15] S. Pega, C. Boissière, D. Grosso, T. Azaïs, A. Chaumonnot, C. Sanchez, Angew. Chem. Int. Ed. 48 (2009) 2784.
[16] C. Chizallet, P. Raybaud, Angew. Chem. Int. Ed. 48 (2009) 2891.
[17] C. Chizallet, P. Raybaud, ChemPhysChem 11 (2010) 105.
[18] O. Cairon, Phys. Chem. Chem. Phys. 12 (2010) 6333.
[19] E.J.M. Hensen, D.G. Poduval, P.C.M.M. Magusin, A.E. Coumans, J.A.R. van Veen, J. Catal. 269 (2010) 201.
[20] E.J.M. Hensen, D.G. Poduval, D.A.J.M. Ligthart, J.A.R. van Veen, M.S. Rigutto, J. Phys. Chem. C 114 (2010) 8363–8374.
[21] D.G. Poduval, J.A.R. van Veen, M.S. Rigutto, E.J.M. Hensen, Chem. Commun. 46 (2010) 3466.
[22] J. Huang, N. van Vegten, Y. Jiang, M. Hunger, A. Baiker, Angew. Chem. Int. Ed. 49 (2010) 7776.
[23] V. Dufaud, J.M. Basset, Angew. Chem. Int. Ed. 37 (1998) 806.
[24] M. Jezequel, V. Dufaud, M.J. Ruiz-Garcia, F. Carrillo-Hermosilla, U. Neugebauer, G.P. Niccolai, F. Lefebvre, F. Bayard, J. Corker, S. Fiddy, J. Evans, J.P. Broyer, J. Malinge, J.M. Basset, J. Am. Chem. Soc. 123 (2001) 3520.
[25] C. Thieuleux, A. Maraval, L. Veyre, C. Copéret, D. Soulivong, J.M. Basset, G.J. Sunley, Angew. Chem. Int. Ed. 46 (2007) 2288.
[26] K. Motokura, M. Tada, Y. Iwasawa, J. Am. Chem. Soc. 129 (2007) 9540.
[27] A.W. Moses, C. Raab, A.E. Nelson, H.D. Leifeste, N.A. Ramsahye, S. Chattopadhyay, J. Eckert, B.F. Chmelka, S.L. Scott, J. Am. Chem. Soc. 129 (2007) 8912.
[28] G.W. Huber, R.D. Cortright, J.A. Dumesic, Angew. Chem. Int. Ed. 43 (2004) 1549.
[29] J.Q. Bond, D.M. Alonso, D. Wang, R.W. West, J.A. Dumesic, Science 327 (2010) 1110.
[30] R.J. Pellet, C.S. Blackwell, J.A. Rabo, J. Catal. 114 (1988) 71.
[31] D. Barthomeuf, Zeolites 10 (1990) 131.
[32] O. Cairon, T. Chevreau, J.C. Lavalley, J. Chem. Soc., Faraday Trans. 94 (1998) 3039.
[33] S.M.C. Menezes, V.L. Camorim, Y.L. Lam, R.A.S. San Gil, A. Bailly, J.P. Amoureux, Appl. Catal. A 207 (2001) 367.
[34] A. Omegna, R. Prins, J.A. van Bokhoven, J. Phys. Chem. B 109 (2005) 9280.
[35] Y. Aoki, H. Habazaki, T. Kunitake, J. Am. Chem. Soc. 131 (2009) 14399.
[36] A. Corma, V. Fornes, M.T. Navarro, J. Perez-Pariente, J. Catal. 148 (1994) 569.

[37] S. Morin, P. Ayrault, S. El Mouahid, N.S. Gnep, M. Guisnet, Appl. Catal. A 159 (1997) 317.
[38] K. Gora-Marek, M. Derewinski, P. Sarv, J. Datka, Catal. Today 101 (2005) 131.
[39] K. Gora-Marek, J. Datka, Appl. Catal. A 302 (2006) 104.
[40] M. Trombetta, G. Busca, M. Lenarda, L. Storaro, M. Pavan, Appl. Catal. A 182 (1999) 225.
[41] M.F. Williams, B. Fonfé, C. Sievers, A. Abraham, J.A. van Bokhoven, A. Jentys, J.A.R. van Veen, J.A. Lercher, J. Catal. 251 (2007) 485.
[42] M. Bevilacqua, T. Montanari, E. Finocchio, G. Busca, Catal. Today 116 (2006) 132.
[43] E. Finocchio, G. Busca, S. Rossini, U. Cornaro, V. Piccoli, R. Miglio, Catal. Today 33 (1997) 335.
[44] B. Xu, C. Sievers, J.A. Lercher, J.A.R. van Veen, P. Giltay, R. Prins, J.A. van Bokhoven, J. Phys. Chem. C 111 (2007) 12075.
[45] B.P. Nielsen, J.H. Onuferko, B.C. Gates, Ind. Eng. Chem. Fundam. 25 (1986) 337.
[46] E. Garrone, B. Onida, B. Bonelli, C. Busco, P. Ugliengo, J. Phys. Chem. B 110 (2006) 19087.
[47] H.A. Benesi, J. Catal. 28 (1973) 176.
[48] P.A. Jacobs, C.F. Heylen, J. Catal. 34 (1974) 267.
[49] L. Oliviero, A. Vimont, J.C. Lavalley, F. Romero Sarria, M. Gaillard, F. Maugé, Phys. Chem. Chem. Phys. 7 (2005) 1861.
[50] I.S. Pieta, M. Ishaq, R.P.K. Wells, J.A. Anderson, Appl. Catal. A 390 (2010) 127.
[51] C. Morterra, G. Cerrato, G. Meligrana, Langmuir 17 (2001) 7053.
[52] T. Onfroy, G. Clet, M. Houalla, Micropor. Mesopor. Mater. 82 (2005) 99.
[53] M. Digne, P. Sautet, P. Raybaud, P. Euzen, H. Toulhoat, J. Catal. 211 (2002) 1.
[54] M. Digne, P. Sautet, P. Raybaud, P. Euzen, H. Toulhoat, J. Catal. 226 (2004) 54.
[55] F. Tielens, C. Gervais, J.F. Lambert, F. Mauri, D. Costa, Chem. Mater. 20 (2008) 3336.
[56] G. Kresse, J. Hafner, Phys. Rev. B 49 (1994) 14251.
[57] G. Kresse, J. Furthmüller, Phys. Rev. B 54 (1996) 11169:1.
[58] J. Perdew, Y. Wang, Phys. Rev. B 45 (1992) 13244.
[59] G. Kresse, D. Joubert, Phys. Rev. B 59 (1999) 1758.
[60] B. Lindberg, J. Chem. Phys. 88 (1988) 3805.
[61] I.N. Senchenya, E. Garrone, P. Ugliengo, J. Mol. Struct. 368 (1996) 93.
[62] P. Ugliengo, in: ANHARM (Eds.), A Program to Solve Numerically the Monodimensional Nuclear Schrödinger Equation, unpublished.
[63] M.R. Basila, T.R. Kantner, K.H. Rhee, J. Phys. Chem. 68 (1964) 3197.
[64] C. Dorémieux-Morin, P. Batamack, C. Martin, J.M. Brégeault, J. Fraissard, Catal. Lett. 9 (1991) 403.
[65] P. Iengo, M. Di Serio, V. Solinas, D. Gazzoli, G. Salvio, E. Santacesaria, Appl. Catal. A 170 (1998) 225.
[66] R. Wischert, C. Copéret, F. Delbecq, P. Sautet, Angew. Chem. Int. Ed. 50 (2011) 3202.
[67] S. Nosé, Prog. Theor. Phys. Suppl. 103 (1991) 1.
[68] T. Demuth, J. Hafner, L. Benco, H. Toulhoat, J. Phys. Chem. B 104 (2000) 4593.
[69] M. Digne, P. Raybaud, P. Sautet, D. Guillaume, H. Toulhoat, J. Am. Chem. Soc. 130 (2008) 11030.
[70] B.A. Morrow, A.J. McFarian, J. Phys. Chem. 96 (1992) 1395.
[71] W. Langel, M. Parrinello, J. Chem. Phys. 103 (1995) 3240.
[72] C. Chizallet, G. Costentin, M. Che, F. Delbecq, P. Sautet, J. Am. Chem. Soc. 129 (2007) 6442.
[73] A. Novak, Struct. Bonding (Berlin) 18 (1974) 177.
[74] H.D. Lutz, Struct. Bonding 69 (1988) 97.
[75] Y. Jeanvoine, J.G. Angyan, G. Kresse, J. Hafner, J. Phys. Chem. B 102 (1998) 5573.
[76] T. Bucko, L. Benco, T. Demuth, J. Hafner, J. Chem. Phys. 117 (2002) 7295.
[77] C. Chizallet, M. Digne, C. Arrouvel, P. Raybaud, F. Delbecq, G. Costentin, M. Che, P. Sautet, H. Toulhoat, Top. Catal. 52 (2009) 1005.
[78] A.G. Pelmenschikov, V.I. Pavlov, G.M. Zhidomirov, S. Beran, J. Phys. Chem. 91 (1987) 3325.
[79] P. O'Malley, J. Dwyer, J. Phys. Chem. 92 (1988) 3005.
[80] U. Eichler, M. Brändle, J. Sauer, J. Phys. Chem. B 101 (1997) 10035.
[81] A. Redondo, P.J. Hay, J. Phys. Chem. 97 (1993) 11754.
[82] J. Macht, M.J. Janik, M. Neurock, E. Iglesia, Angew. Chem. Int. Ed. 46 (2007) 7864.
[83] J. Macht, R.T. Carr, E. Iglesia, J. Am. Chem. Soc. 131 (2009) 6554.
[84] X. Rozanska, R. van Santen, F. Hutschka, J. Hafner, J. Am. Chem. Soc. 123 (2001) 7655.
[85] M. Castella-Ventura, Y. Akacem, E. Kassab, J. Phys. Chem. C 112 (2008) 19045.
[86] DMol3 is accessible through the Materials Studio 6.0 interface commercialized by Accelrys Inc.
[87] J. Védrine, D. Barthomeuf, G. Dalmai, Y. Trambouze, B. Imelik, M. Prettre, C. R. Acad. Sci. Paris 267 (1968) 118.
[88] J.F. Stebbins, P. McMillan, Am. Mineral. 74 (1989) 965.
[89] J.F. Stebbins, Nature 351 (1991) 638.
[90] S.J. Gaudio, S. Sen, C.E. Lesher, Geochim. Cosmochim. Acta 72 (2008) 1222.
[91] H. Koller, A. Wölker, H. Eckert, C. Panz, P. Behrens, Angew. Chem. Int. Ed. 36 (1997) 2823.
[92] M.A. Camblor, M.J. Diaz-Cabanas, J. Perez-Pariente, S.J. Teat, W. Clegg, I.J. Shannon, P. Lightfoot, P.A. Wright, R.E. Morris, Angew. Chem. Int. Ed. 37 (1998) 2122.
[93] I. Bull, L.A. Villaescusa, S.J. Teat, M.A. Camblor, A.F. Wright, P. Lightfoot, R.E. Morris, J. Am. Chem. Soc. 122 (2000) 7128.
[94] C.A. Fyfe, D.H. Brouwer, A.R. Lewis, J.M. Chézeau, J. Am. Chem. Soc. 123 (2001) 6882.
[95] G. Hartmeyer, C. Marichal, B. Lebeau, B. Caullet, J. Hernandez, J. Phys. Chem. C 111 (2007) 6634.
[96] C. Chuit, R.J.P. Corriu, C. Reye, J.C. Young, Chem. Rev. 93 (1993) 1371.
[97] R.R. Holmes, Chem. Rev. 96 (1996) 927.
[98] S. Metz, C. Burschka, D. Platte, R. Tacke, Angew. Chem. Int. Ed. 46 (2007) 7006.
[99] S.E. Johnson, J.A. Deiters, R.O. Day, R.R. Holmes, J. Am. Chem. Soc. 111 (1989) 3250.
[100] J.L. Brefort, R.J.P. Corriu, C. Guerin, B.J.L. Henner, W.W.C.W.C. Man, Organometallics 9 (1990) 2080.
[101] A. Mix, U.H. Berlekamp, H.G. Stammler, B. Neumann, P. Jutzi, J. Organomet. Chem. 521 (1996) 177.
[102] M. Spiniello, J. White, Organometallics 27 (2008) 994.
[103] K.C. Kumara Swamy, V. Chandrasekhar, J.J. Harland, J.M. Holmes, R.O. Day, R.R. Holmes, J. Am. Chem. Soc. 112 (1990) 2341.
[104] K.Y. Blohowiak, D.R. Treadwell, B.L. Mueller, M.L. Hoppe, S. Jouppi, P. Kansal, K.W. Chew, C.L.S. Scotto, F. Babonneau, J. Kampf, R.M. Laine, Chem. Mater. 6 (1994) 2177.
[105] J.F. Stebbins, P. McMillan, J. Non-Cryst. Solids 160 (1993) 116.
[106] B. Herreros, S.W. Carr, J. Klinowski, Nature 263 (1994) 1585.
[107] S.D. Kinrade, J.W. Del Nin, A.S. Scach, T.A. Sloan, K.L. Wilson, C.T.G. Knight, Science 285 (1999) 1542.
[108] M.R. Gallas, G.J. Piermarini, J. Am. Ceram. Soc. 77 (1994) 2917.
[109] R.T. Downs, D.C. Palmer, Am. Mineral. 79 (1994) 9.
[110] T. Demuth, X. Rozanska, L. Benco, J. Hafner, R. van Santen, H. Toulhoat, J. Catal. 214 (2003) 68.
[111] C. Tuma, J. Sauer, Angew. Chem. Int. Ed. 44 (2005) 4769.
[112] M. Boronat, A. Corma, Appl. Catal. A 336 (2008) 2.